Article

Cell Chemical Biology

Mechanism by which a linoleic acid metabolite suppresses cancer cell growth by inhibiting mTOR

Graphical abstract

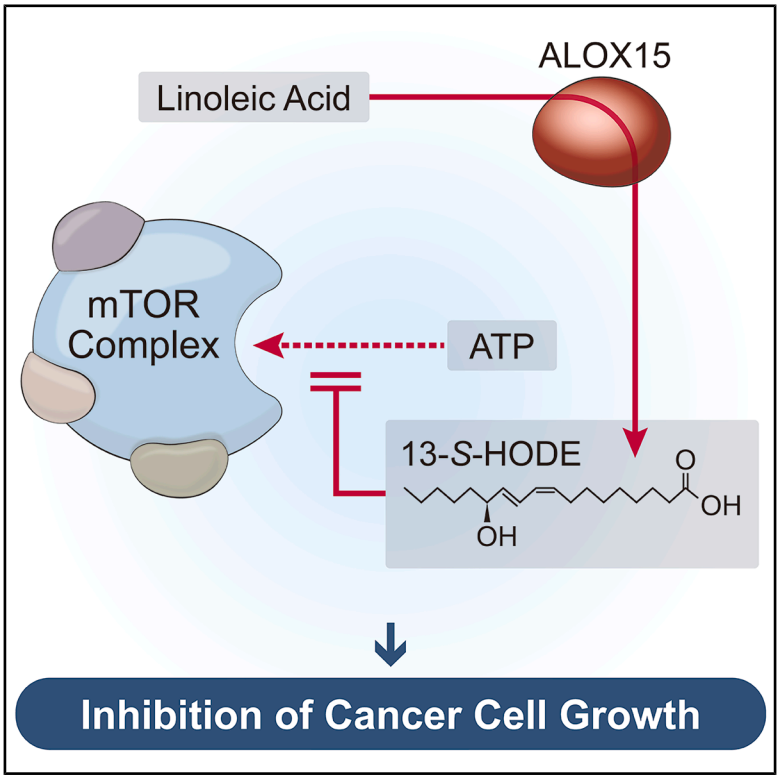

Authors

Seung Ju Park, Sera Kim, Hongmok Kwon, ..., Mi-Young Kim, Youngjoo Byun, Seyun Kim

Correspondence

yjbyun1@korea.ac.kr (Y.B.), seyunkim@kaist.ac.kr (S.K.)

In brief

Cell growth is controlled by mTOR signaling, but how metabolism directly regulates this pathway is unclear. Park and Kim et al. identify the linoleic acid metabolite 13-*S*-HODE as an endogenous inhibitor of mTOR, linking polyunsaturated fatty acid metabolism to the suppression of cancer cell and tumor growth.

Highlights

- Identify 13-*S*-hydroxyoctadecadeinoic acid (13-*S*-HODE) as mTOR-interacting metabolite
- 13-*S*-HODE directly targets the mTOR kinase domain as an ATP-competitive inhibitor
- 13-*S*-HODE inhibits mTOR signaling and cancer cell growth
- ALOX15 overexpression reduces mTOR signaling and cancer cell growth

Park et al., 2026, Cell Chemical Biology *33*, 637–648
May 21, 2026
https://doi.org/10.1016/j.chembiol.2026.04.004

CellPress

Cell Chemical Biology

CellPress

Article

Mechanism by which a linoleic acid metabolite suppresses cancer cell growth by inhibiting mTOR

Seung Ju Park,[1,8,9] Sera Kim,[1,8] Hongmok Kwon,[2] Jiyeon Choi,[1,10] Ji Kwang Kim,[1] Inhong Jung,[1] Seol-Wa Lim,[1,9] Young Ran Kim,[1] A-Yeong Yang,[1] Boah Lee,[1,9] Haein Lee,[1,11] Seung Eun Park,[1] Seulgi Lee,[1,9] Myeongsu Shin,[2] Bernie Byunghoon Park,[2] YunHye Kim,[2] Jinwook Lee,[3] Byung-Chul Oh,[3] Daniel Deredge,[4] Patrick L. Wintrode,[4] Mi-Young Kim,[1] Youngjoo Byun,[2,5,*] and Seyun Kim[1,6,7,12,*]

[1]Department of Biological Sciences, Korea Advanced Institute of Science and Technology (KAIST), Daejeon, Republic of Korea
[2]College of Pharmacy, Korea University, Sejong, Republic of Korea
[3]Department of Physiology, Lee Gil Ya Cancer and Diabetes Institute, Gachon University, College of Medicine, Incheon, Republic of Korea
[4]Department of Pharmaceutical Sciences, University of Maryland School of Pharmacy, Baltimore, MD, USA
[5]Interdisciplinary Major Program in Innovative Pharmaceutical Sciences, Korea University, Sejong, Republic of Korea
[6]KAIST Institute for the BioCentury, KAIST, Daejeon, Republic of Korea
[7]KAIST Stem Cell Center, KAIST, Daejeon, Republic of Korea
[8]These authors contributed equally
[9]Present address: ERSTEQ co., Ltd, Daejeon, Republic of Korea
[10]Present address: LigaChem Biosciences Inc, Daejeon, Republic of Korea
[11]Present address: Department of Ecology, Evolution and Marine Biology, University of California Santa Barbara, Santa Barbara, California, USA
[12]Lead contact
*Correspondence: yjbyun1@korea.ac.kr (Y.B.), seyunkim@kaist.ac.kr (S.K.)
https://doi.org/10.1016/j.chembiol.2026.04.004

SIGNIFICANCE Mechanistic target of rapamycin (mTOR) is a key protein kinase that integrates various signals to control cell growth. Despite complex networks of mTOR with mTOR-associated proteins, endogenous cellular metabolites capable of interacting with mTOR have largely remained elusive. We identified that 13-*S*-hydroxyoctadecadienoic acid (13-*S*-HODE), a bioactive oxygenated metabolite of linoleic acid, a polyunsaturated essential fatty acid, directly binds to the catalytic domain of mTOR, thereby inhibiting its kinase activity. Either 13-*S*-HODE treatment or expression of arachidonate 15-lipoxygenase, an enzyme responsible for 13-*S*-HODE production, reduces mTOR and its downstream signaling activities, thus suppressing the growth of cancer cells as well as tumor xenografts. Thus, our data propose 13-*S*-HODE as a tumor suppressive, mTOR-inhibiting cellular metabolite involved in controlling cancer cell growth.

SUMMARY

Mechanistic target of rapamycin (mTOR) is a key protein kinase that integrates various internal and external signals to control biological events including cell growth. Whereas substantial efforts were made to elucidate protein subunits interacting with mTOR, endogenous metabolite-mTOR interactions remain largely unknown. Using affinity protein purification and mass spectrometry, we identified direct binding of mTOR to 13-*S*-hydroxyoctadecadienoic acid (13-*S*-HODE) which is an oxygenated metabolite of linoleic acid, a polyunsaturated essential fatty acid. Interaction of 13-*S*-HODE with the catalytic ATP-binding domain of mTOR prevented its kinase activity in an ATP-competitive manner. Furthermore, either 13-*S*-HODE treatment or expression of arachidonate 15-lipoxygenase (ALOX15), an enzyme responsible for 13-*S*-HODE production, reduced mTOR signaling, thereby suppressing the growth of cancer cells as well as tumor xenografts. Our results highlight the importance of 13-*S*-HODE serving as a tumor suppressive, mTOR-inhibiting metabolite that links polyunsaturated fatty acid metabolism and the mTOR signaling in controlling cancer cell growth.

INTRODUCTION

Multiple mechanisms have evolved to sense fluctuations in a wide range of cellular small molecules, including nutrients and their modified metabolites, to coordinate signaling networks.[1–3] Elucidating the molecular interactions among macromolecules and small molecules is essential for fully uncovering signaling networks.[4–6] Recently, although small metabolite regulators of

proteins have become the significant focus of attention, a limited number of metabolite-protein interactions have been identified relative to other extensive protein-protein and protein-nucleic acid interaction networks.[4,7,8]

Mechanistic target of rapamycin (mTOR) is a key signaling node integrating various environmental signals from growth factors, stress, and nutrients to control major biological events such as growth and metabolism.[9–11] Major efforts to understand mTOR-binding proteins has allowed us to define two multiprotein complexes, mTOR complex 1 (mTORC1) and 2 (mTORC2): mTORC1 controls cellular growth by phosphorylating S6 kinase 1 (S6K1), whereas mTORC2 regulates cell survival by phosphorylating Akt (also known as protein kinase B) and serum/glucocorticoid regulated kinase 1 (SGK1).[10,12–14] It is clear that the dysregulation of the mTOR signaling pathway occurs in many human diseases, including cancer.[15,16] Importantly, it has been found that majority of human cancers are associated with aberrant activation of mTOR.[17–19] Thus, dissecting the mTOR-controlling molecular pathways could offer new insights into a better understanding of the mTOR signaling networks and the development of mTOR-targeting therapeutics. Numerous protein factors that physically interact with mTOR and regulate its activity have been identified (e.g., raptor [regulatory-associated protein of mTOR], rictor [rapamycin-insensitive companion of mTOR], DEPTOR [DEP domain-containing mTOR-interacting protein], and PRAS40 [proline-rich Akt substrate of 40 kDa]),[12,13,20–22] whereas phosphatidic acid is the only endogenous metabolite proposed to bind and stimulate mTORC1.[23] However, identifying other cellular metabolites that may interact with mTOR and its associated pathways remains to be established.

Herein, we identify 13-*S*-hydroxyoctadecadienoic acid (13-*S*-HODE), an oxidized linoleic acid metabolite (OXLAM), as an mTOR-associated small molecule. Mechanistically, 13-*S*-HODE directly binds to the catalytic domain of mTOR, thereby acting to inhibit mTOR kinase in an ATP-competitive manner. Consequently, 13-*S*-HODE treatment or overexpression of ALOX15 led to the suppressed mTOR signaling, decreased proliferation, and reduced the growth of cultured cancer cells and tumor xenografts. Collectively, our findings reveal that 13-*S*-HODE as a tumor-suppressive polyunsaturated fatty acid (PUFA) metabolite, plays a key role in inhibiting mTOR, thereby suppressing cancer cell growth.

RESULTS

Affinity protein purification and mass spectrometry reveals 13-*S*-HODE as an mTOR-associated metabolite

To identify mTOR-binding small metabolites, we performed affinity protein purification followed by liquid chromatography-mass spectrometry (LC-MS) (Figure 1A). FLAG-tagged mTOR was overexpressed in human embryonic kidney 293 T (HEK293T) cells and immunopurified. Metabolites extracted from FLAG-mTOR immunoprecipitates were analyzed via LC-MS metabolite profiling based on accurate molecular mass and retention time. A peak ($[M-H]^-$: 295.2264 amu) at 6.51 min in the negative ion mode (Figure 1B) was identified as 13-*S*-HODE, an oxygenated product of linoleic acid,[24] the essential PUFA, on the basis of the same retention time and molecular mass of pure 13-*S*-HODE (Figures 1B, 1C, and S1A). To verify these findings, HEK293 cell lysates were incubated with biotin, biotin-labeled linoleic acid, or biotin-labeled 13-*S*-HODE. The pulldown assay using biotin-linoleic acid showed no binding to mTOR, raptor, or rictor (Figure S1B). Notably, biotin-labeled 13-*S*-HODE bound to mTOR and its complex subunits, raptor and rictor, but was competed off in the presence of unlabeled 13-*S*-HODE (Figure 1D), clearly supporting associations between 13-*S*-HODE and mTOR in cells.

13-*S*-HODE directly inhibits mTOR kinase activity *in vitro*

We examined whether 13-*S*-HODE directly influences mTOR kinase activity to establish the physiological significance of 13-*S*-HODE-mTOR interactions. To address this issue, *in vitro* kinase assays were performed using either raptor or rictor immunoprecipitates prepared from HEK293T cells. 13-*S*-HODE inhibited phosphorylation at T389 of the mTORC1 substrate, S6K1 in a dose-dependent manner (Figure 2A). Incubation with 13-*S*-HODE additionally blocked phosphorylation of the mTORC2 substrate, Akt, at S473 (Figure 2B), indicating inhibitory activity of the metabolite against both mTORC1 and mTORC2. Relative to the concentration of 13-*S*-HODE required for mTORC1 inhibition, a higher amount was needed to achieve the same level of suppression for mTORC2 (Figures 2A, 2B, and S2A), suggesting selective activity toward mTORC1.

For further confirmation of whether 13-*S*-HODE directly interacts with the mTOR kinase domain, we conducted an *in vitro* kinase assay using the recombinant mTOR C-terminal fragment encompassing amino acid residues 1,362 to 2,549 that form the intact kinase domain. Notably, 13-*S*-HODE, but not vehicle, inhibited S6K1 phosphorylation (Figure 2C). 15-*S*-HETE, a minor metabolite generated by arachidonate 15-lipoxygenase (ALOX15), the enzyme responsible for 13-*S*-HODE biosynthesis,[25–28] was further tested and found to inhibit mTOR kinase activity *in vitro* in a manner similar to 13-*S*-HODE (Figure S2B). Importantly, 13-*S*-HODE failed to exert inhibitory effects on other kinases, including phosphatidylinositol 3-kinase-related kinases (e.g., phosphatidylinositol 3-kinase C3, DNA-dependent protein kinase and extracellular signal-regulated kinase) (Figures S2C–S2E), highlighting the selective inhibitory activity of 13-*S*-HODE against mTOR. In pulldown experiments, we further detected interactions of biotin-labeled 13-*S*-HODE with the recombinant mTOR C-terminal region (Figure 2D). This binding was specific, since biotin-labeled linoleic acid used as a control did not interact with the mTOR C-terminal fragment nor inhibit its kinase activity (Figures 2D, 2E, and S1B). Our findings collectively suggest that 13-*S*-HODE inhibits mTOR activity through direct interactions with the kinase domain.

13-*S*-HODE binds to the kinase domain of mTOR and acts as an ATP-competitive inhibitor

To gain insights into the mechanism of action of 13-*S*-HODE and establish the potential binding site, we focused on the structural and conformational consequences of 13-*S*-HODE binding to the mTOR C- terminus with the aid of hydrogen/deuterium exchange MS (HDX-MS). In the presence of 13-*S*-HODE, several regions exhibited altered deuterium uptake kinetics, which predominantly localized to the kinase domain (Figures S3A and S3B).

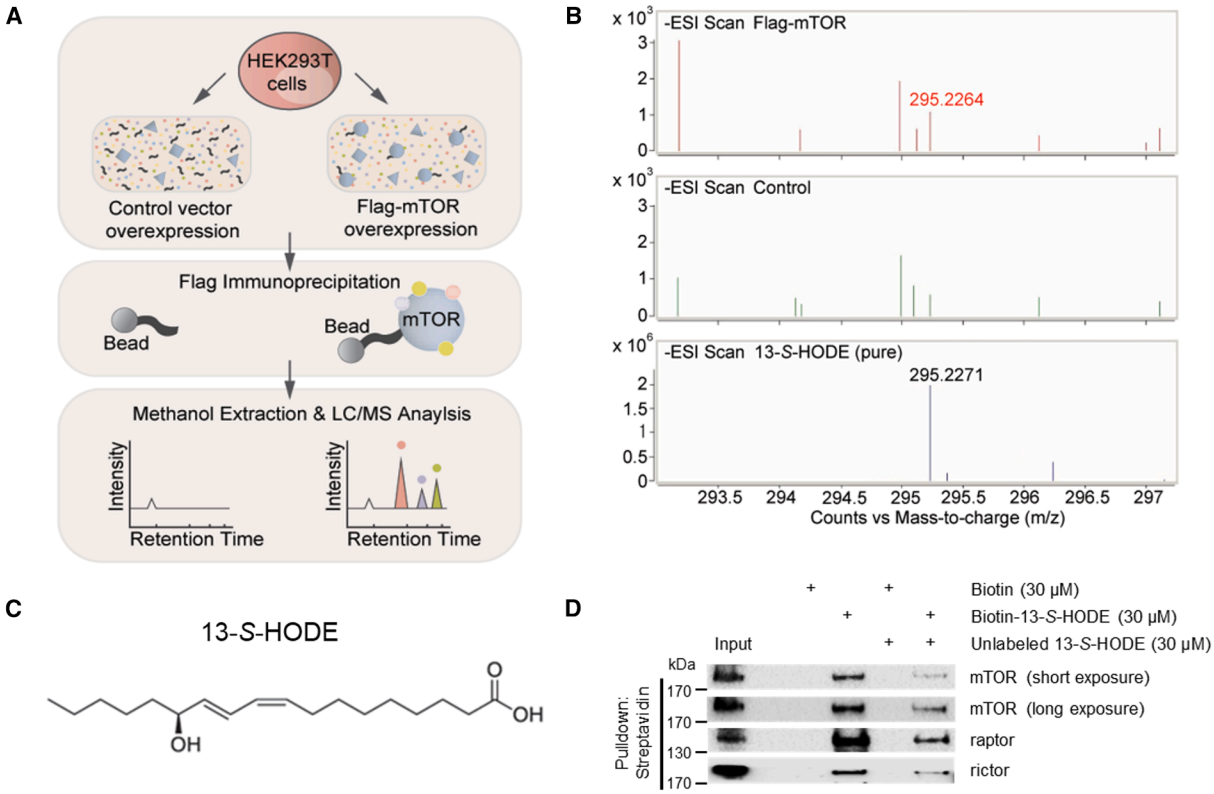

Figure 1. Identification of 13-*S*-HODE as an mTOR-associated metabolite

(A) Experimental schematics for screening endogenous small molecules bound to mTOR. Metabolites specifically bound Flag-mTOR immunoprecipitates relative to control were identified using LC-MS.

(B) Extracted ion chromatographs of FLAG-mTOR (top) and negative control (middle) at 6.51 min in the negative mode. The abundant metabolite ($[M-H]^-$: 295.2264) in FLAG-mTOR was confirmed as 13-*S*-HODE by comparison with accurate determinations of the molecular mass and retention times of pure 13-*S*-HODE ($[M-H]^-$: 295.2271, lower) under the same LC-MS conditions.

(C) Chemical structure of 13-*S*-HODE.

(D) Binding of biotin-labeled 13-*S*-HODE to endogenous mTOR, raptor, or rictor in HEK293T cell lysates assessed via streptavidin bead pulldown and immunoblotting. Blots are representative of three independent experiments.

A more detailed examination revealed that peptides including residues 1,943–1,956 at the linker region between the FAT (FRAP, ATM, and TRRAP) and FKBP12-rapamycin binding (FRB) domains, 2,186–2,196, 2,270–2,280, 2,303–2,314, or 2,421–2,431 of the kinase domain of mTOR displayed a significant decrease in exchange at the earliest experimental time point of D_2O incubation (10 s) (Figures S3C and S3D), suggestive of potential ligand-binding sites. Mapping of protected regions on the crystal structure of mTOR[29] revealed that the potential 13-*S*-HODE binding site spans across the catalytic cleft of the kinase protein (Figure 3A).

Based on these results, we further performed docking simulations of 13-*S*-HODE at the catalytic site of mTOR kinase to elucidate its potential binding mode. The best docked pose of 13-*S*-HODE was located close to the ATP-binding site of the catalytic cleft of mTOR and formed hydrogen bonds with several residues including Lys2187, Glu2190, His2247, His2340, and Ser2342 (Figure 3B). Two of the residues, Lys2187 and Glu2190, were located in areas potentially protected by 13-*S*-HODE according to HDX-MS data (Figures 3A, S3C, and S3D). These amino acids have also been documented as the key interacting residues with the ADP-MgF_3-Mg_2 complex in the mTOR crystal structure,[29] leading to the proposal that 13-*S*-HODE acts as an ATP-competitive inhibitor.

We next tested direct interaction between 13-*S*-HODE and purified mTOR kinase domain. The thermal stability of recombinant mTOR kinase domain was evaluated by varying concentrations of 13-*S*-HODE. We found that 13-*S*-HODE, but not linoleic acid, reduced the thermal stability of recombinant mTOR kinase domain in a concentration-dependent manner, i.e., 30 μM of 13-*S*-HODE decreased the T_m by approximately 2.29 °C (Figures 3C, 3D, and S3E), suggesting that 13-*S*-HODE directly binds to the kinase domain of mTOR. To clarify whether 13-*S*-HODE-mTOR interactions represent a specific event occurring within the ATP-binding pocket of mTOR, we focused on the residues of mTOR required for interactions with 13-*S*-HODE. Based on docking simulation data, $mTOR^{K2187A/E2190A}$ mutants were generated. We analyzed the interaction between the $mTOR^{K2187A/E2190A}$ and 13-*S*-HODE using the cellular thermal shift assay (CETSA). 13-*S*-HODE induced the thermal stability of $mTOR^{WT}$ in a temperature-dependent manner, whereas $mTOR^{K2187A/E2190A}$ failed to exhibit this stabilizing effect

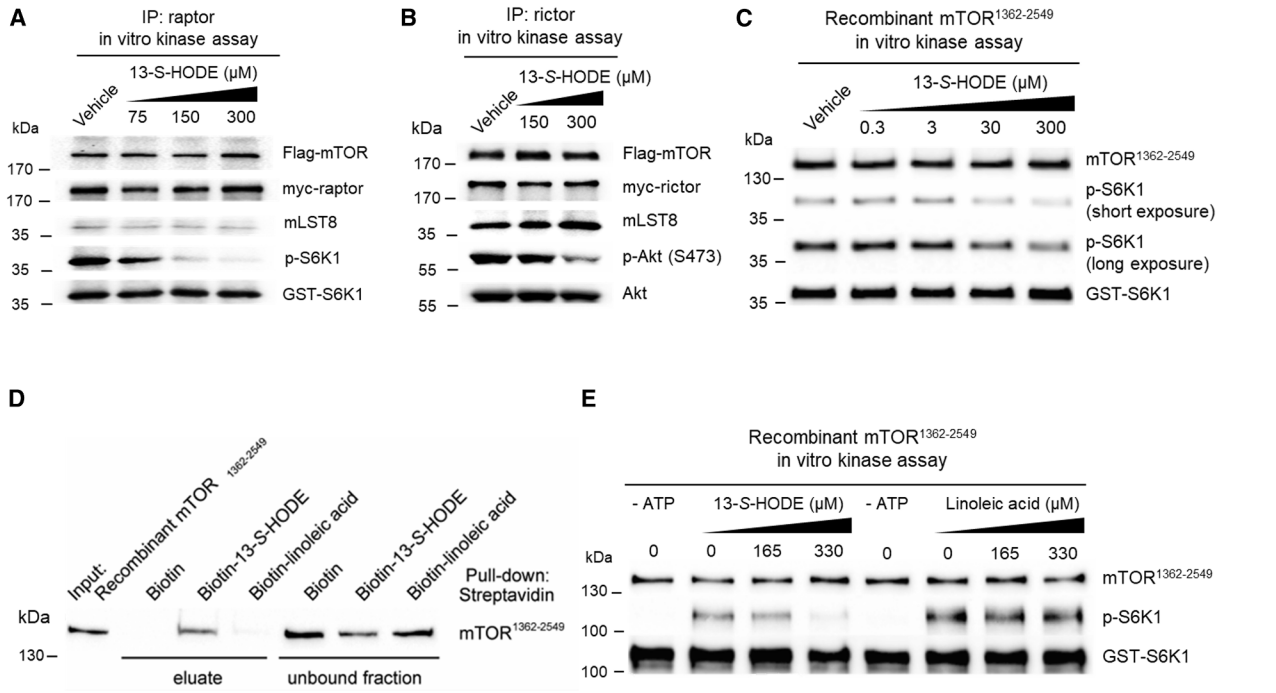

Figure 2. 13-*S*-HODE directly inhibits mTOR kinase activity

(A and B) *In vitro* mTOR kinase assays were performed in the absence or presence of 13-*S*-HODE. FLAG-raptor or FLAG-rictor was cotransfected in HEK293T cells with myc-tagged mTOR. mTORC1 kinase activity was assessed by using FLAG-raptor immunoprecipitates via immunoblotting of T389 S6K1 phosphorylation (A). mTORC2 kinase activity was analyzed by using FLAG-rictor immunoprecipitates, based on S473 Akt phosphorylation (B).

(C) *In vitro* kinase assays were performed using the recombinant human mTOR C-terminal region (mTOR$^{1362-2549}$). mTOR kinase activity was evaluated based on the T389 S6K1 phosphorylation level.

(D) Binding of biotin-labeled 13-*S*-HODE to recombinant mTOR$^{1362-2549}$ was assessed via streptavidin bead pulldown and immunoblotting.

(E) *In vitro* kinase assays were performed using the recombinant human mTOR C-terminal region (mTOR$^{1362-2549}$) in the absence or presence of either linoleic acid or 13-*S*-HODE. All images show representative experiments that were repeated independently three times.

(Figure 3E), confirming that K2187 and E2190 of mTOR are critical for its direct interaction with 13-*S*-HODE. Because K2187 and E2190 are residues essential for ATP binding,[29] mTOR$^{K2187A/E2190A}$ lacks intrinsic kinase activity (Figure S3F); therefore, it was not possible to assess whether 13-*S*-HODE inhibits mTOR activity using this mutant. The potential ATP-competitive mechanism of 13-*S*-HODE was further investigated by performing an *in vitro* mTOR kinase assay in the presence of 13-*S*-HODE along with various concentrations of ATP. Notably, the inhibitory effect of 13-*S*-HODE on mTOR was abolished with increasing ATP concentrations (Figure 3F), validating 13-*S*-HODE action through an ATP-competitive mechanism.

13-*S*-HODE inhibits mTOR signaling and cancer cell growth

In multiple human cancer types, nearly undetectable levels of 13-*S*-HODE and arachidonate 15-lipoxygenase (*ALOX15*), a rate-limiting enzyme that synthesizes 13-*S*-HODE from linoleic acid have been reported,[25–28] suggesting a crucial role of 13-*S*-HODE as a tumor suppressive metabolite. However, the effect of 13-*S*-HODE on mTOR signaling has not yet been profoundly investigated. Colorectal cancer (CRC) cell lines (HT-29 and SW480) were assessed to test the role of 13-*S*-HODE in cellular mTOR signaling events. Treatment of the CRC cells with 13-*S*-HODE for 48 h reduced phosphorylation at T389 of S6K1 and S240/244 of S6 but not S473 of Akt (Figure 4A), thereby demonstrating 13-*S*-HODE's inhibitory effect on mTORC1. Similar mTORC1 inhibition was observed in other cancer cells such as MDA-MB-468 breast cancer cells and U-373 MG glioblastoma, as shown by the decreased phosphorylation of S6K1 and S6 upon treatment with 13-*S*-HODE (Figure 4B). Acute 30-min treatment with 13-*S*-HODE did not produce a detectable inhibitory effect on mTOR signaling (Figure S4A). In addition, the treatment of MDA-MB-468 cells with 13-*S*-HODE resulted in reduced proliferation (Figure 4C) and colony formation (Figure 4D). When normal cell lines, such as MCF10A and NCM460D, were tested, corresponding cancer cells (e.g., MDA-MB-468, SW480) exhibited a greater reduction in cell viability upon 13-*S*-HODE treatment, indicating that 13-*S*-HODE selectively reduces the viability of cancer cells relative to normal cells (Figures S4B and S4C). The effects of 13-*S*-HODE on tumor growth *in vivo* were examined by injecting MDA-MB-468 cells subcutaneously into immunocompromised mice and monitoring tumor growth. The growth of MDA-MB-468 xenografts was significantly inhibited by 13-*S*-HODE administration (Figures 4E and 4F), thus confirming its anti-cancer effects *in vivo*.

13-*S*-HODE suppresses mTOR signaling and the growth of cancer cells with hyperactive *MTOR* mutation

Recently, gain-of-function *MTOR* mutations have been discovered from several types of cancers and serve as biomarkers to

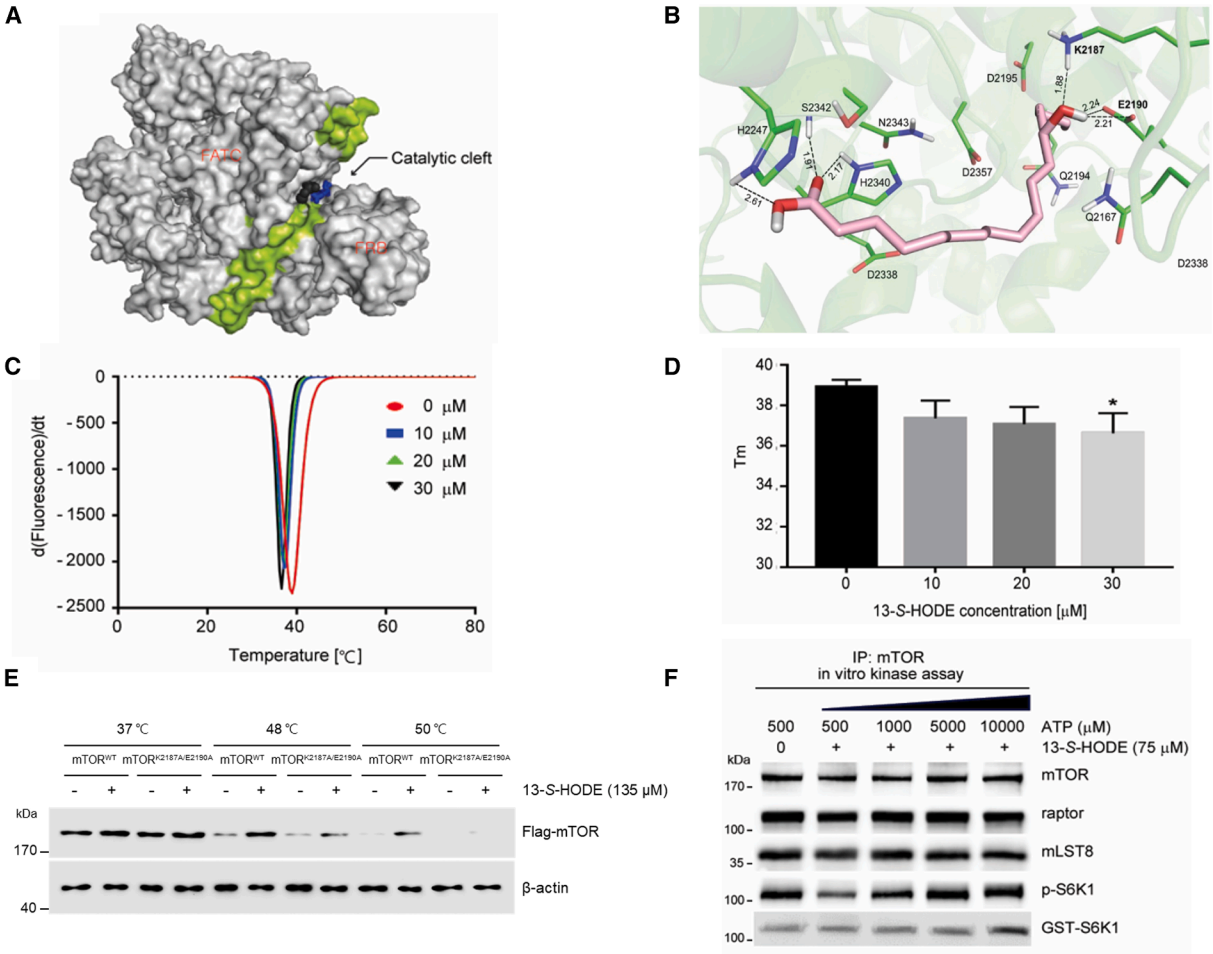

Figure 3. 13-*S*-HODE acts as an ATP-competitive inhibitor

(A) Peptides showing significant deviation were mapped onto the structure of mTOR (PDB: 4JSV) on a surface representation. Regions with a significant decrease in deuterium uptake in the presence of 13-*S*-HODE are colored green. Magnesium ions are presented in a black sphere and ADP is labeled in blue to highlight the catalytic site.

(B) Optimal docking pose of 13-*S*-HODE in the catalytic site of mTOR kinase. Hydrogen bond interactions between 13-*S*-HODE and mTOR were observed (OH group of 13-HODE with Lys2197 and Glu2190, COOH group with His2340, Ser2342, and His2247). The numbers indicate intermolecular hydrogen bond distance in Å.

(C and D) The thermal denaturation of recombinant mTOR kinase domain was measured in the absence and presence of varying 13-*S*-HODE concentrations, as indicated. Representative derivative (dF/dT) curves are shown for untreated and treated with varying ligand concentrations (C). Midpoint temperatures of the protein-unfolding transition (T_m) are presented as bars (D).

Data are mean ± SD of at least three independent measurements (*$p < 0.05$).

(E) CETSA was carried out to evaluate the thermal stability of 13-*S*-HODE-bound mTOR. HEK293T cells were transfected with FLAG-mTOR^{WT} or FLAG-mTORK$^{2187A/E2190A}$. Cell lysates were incubated with 13-*S*-HODE for 1 h at 4°C. Actin was used as a nontarget protein.

(F) *In vitro* mTORC1 activity of raptor immunoprecipitates prepared from HEK293 cells assayed in the presence of 75 μM 13-*S*-HODE and increasing concentrations of ATP.

T389 phosphorylation of S6K1 was measured via immunoblotting. Representative experiments are shown, which were repeated independently three times (E and F), all with similar results.

predict their responses to mTOR inhibitors.[30] Based on our findings that 13-*S*-HODE inhibits mTOR, we put forward the hypothesis that 13-*S*-HODE could retard the growth of cancer cells with a hyperactive *MTOR* mutation. To examine this possibility, we selected JHUEM7 endometrial cancer cells harboring the mTORC1-activating *MTOR* mutation S2215Y[30]; 13-*S*-HODE treatment resulted in decreased proliferation as well as colony formation of JHUEM7 cells (Figures 5A, 5B, and S5A). As it has been reported for other cancer cells,[31,32] endogenous 13-*S*-HODE was almost undetectable in vehicle treated JHUEM7 cells, whereas it was approximately 150 μM in JHUEM7 cells treated with 13-*S*-HODE for 48 h (Figure S5B), thereby confirming efficient intracellular uptake of 13-*S*-HODE. Notably, treatment with 13-*S*-HODE also suppressed cell viability in HeLa cells, which do not harbor hyperactivating *MTOR* mutations (Figure S5C), indicating that sensitivity to 13-S-HODE is not restricted to cancer cells with constitutively active mTOR. To investigate the effects of 13-*S*-HODE on global gene expression in JHUEM7 cells, we performed

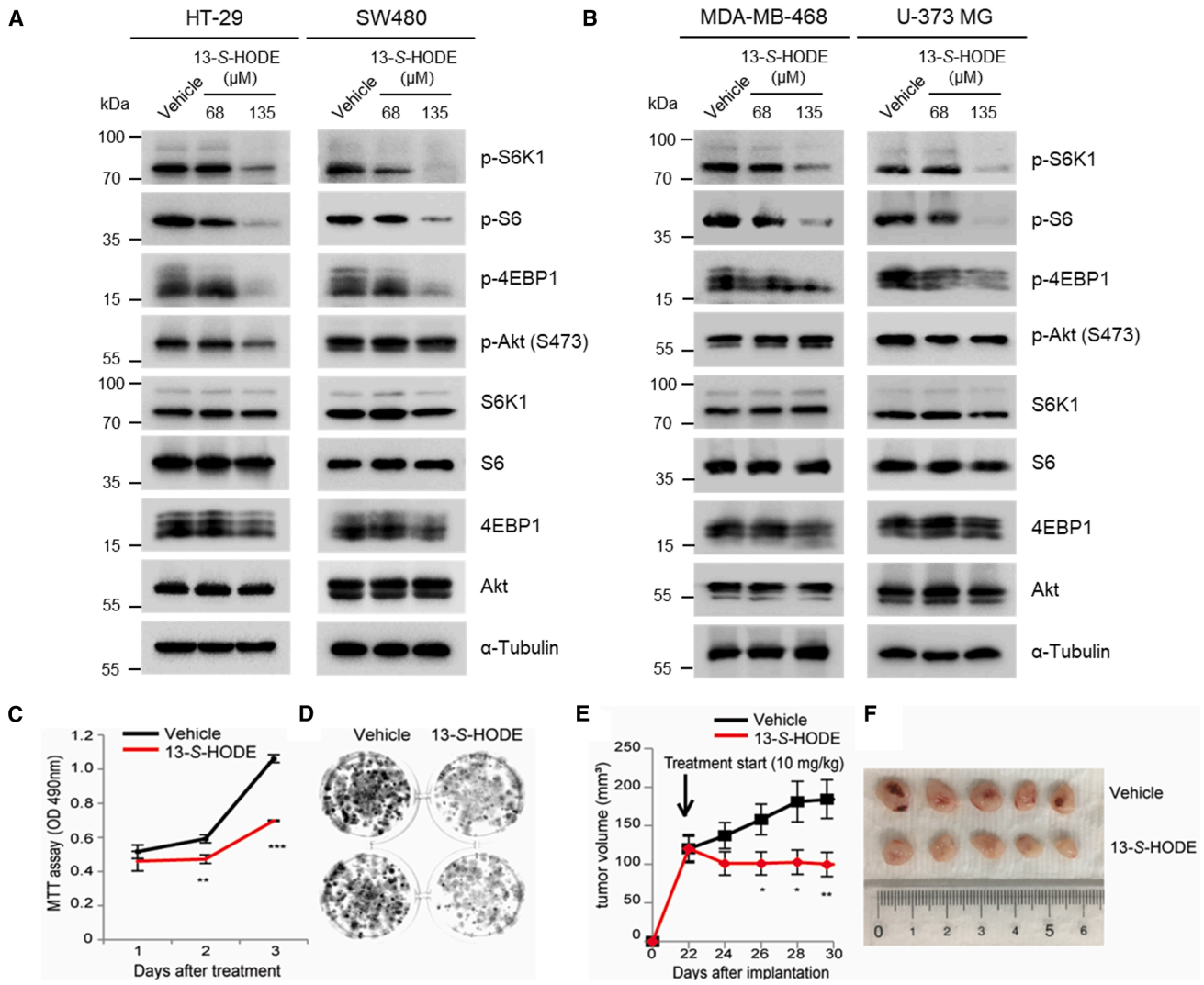

Figure 4. 13-*S*-HODE inhibits mTOR signaling and cancer cell growth

(A) HT-29, SW480 colorectal cancer cells were treated with DMSO vehicle or 13-*S*-HODE for 48 h. Cell lysates were analyzed by immunoblotting for the levels of the indicated proteins and phosphorylation states.

(B) MDA-MB-468 breast cancer cells and U-373 MG glioblastoma cells were treated with DMSO vehicle or 13-*S*-HODE for 48 h. Cell lysates were analyzed by immunoblotting for the levels of the indicated proteins and phosphorylation states.

(C and D) Cell viability (C) and colony formation (D) of DMSO vehicle or 135 μM 13-*S*-HODE treated MDA-MB-468 cells were measured.

Data are expressed as mean ± SEM (*$p < 0.05$; **$p < 0.01$; ***$p < 0.001$, Student's *t* test.).

(E and F) MDA-MB-468 cells were inoculated into flanks of nude mice ($n = 6$ per group) and tumor volumes were measured for 30 days after injection. DMSO vehicle or 13-*S*-HODE (10 mg/kg) were intratumorally injected five times into xenograft tumors every 2 days (E).

Data are expressed as mean ± SE (*$p < 0.05$, **$p < 0.01$, ***$p < 0.001$, Student's *t* test.).

Representative images of xenograft tumors at the day of sacrifice (F).

RNA sequencing. 13-*S*-HODE treatment downregulated 3,729 genes and up-regulated 3,842 genes (Figure 5C). Specifically, according to KEGG pathway enrichment analyses (Figures S5D and S5E), genes in the mTOR signaling pathway were markedly altered by 13-*S*-HODE treatment, which supports its action in the mTOR pathway. Significant changes in gene sets linked to various cancer-related pathways further suggest 13-*S*-HODE's anti-cancer activity (Figure S5D).

Next, we found that 13-*S*-HODE treatment reduced phosphorylation at T389 of S6K1 but not S473 of Akt (Figure 5D), thereby validating potent mTORC1 inhibition by 13-*S*-HODE. As shown in an mTOR kinase assay (Figures 2A and 2B), mTORC1 appears more sensitive to 13-*S*-HODE than mTORC2 (Figure 5D), presumably reflecting structural differences between the two distinct mTOR complexes.[29,33–37] Interestingly, longer treatment of 13-*S*-HODE for 96 h decreased phosphorylation of both S6K1 T389 and Akt S473 (Figure 5E), suggesting that prolonged application of 13-*S*-HODE leads to the inhibition of both mTORC1 and mTORC2 in cells. In our immunoprecipitation mTOR kinase assays using the hyperactive mTOR-mutants $mTOR^{S2115Y}$,

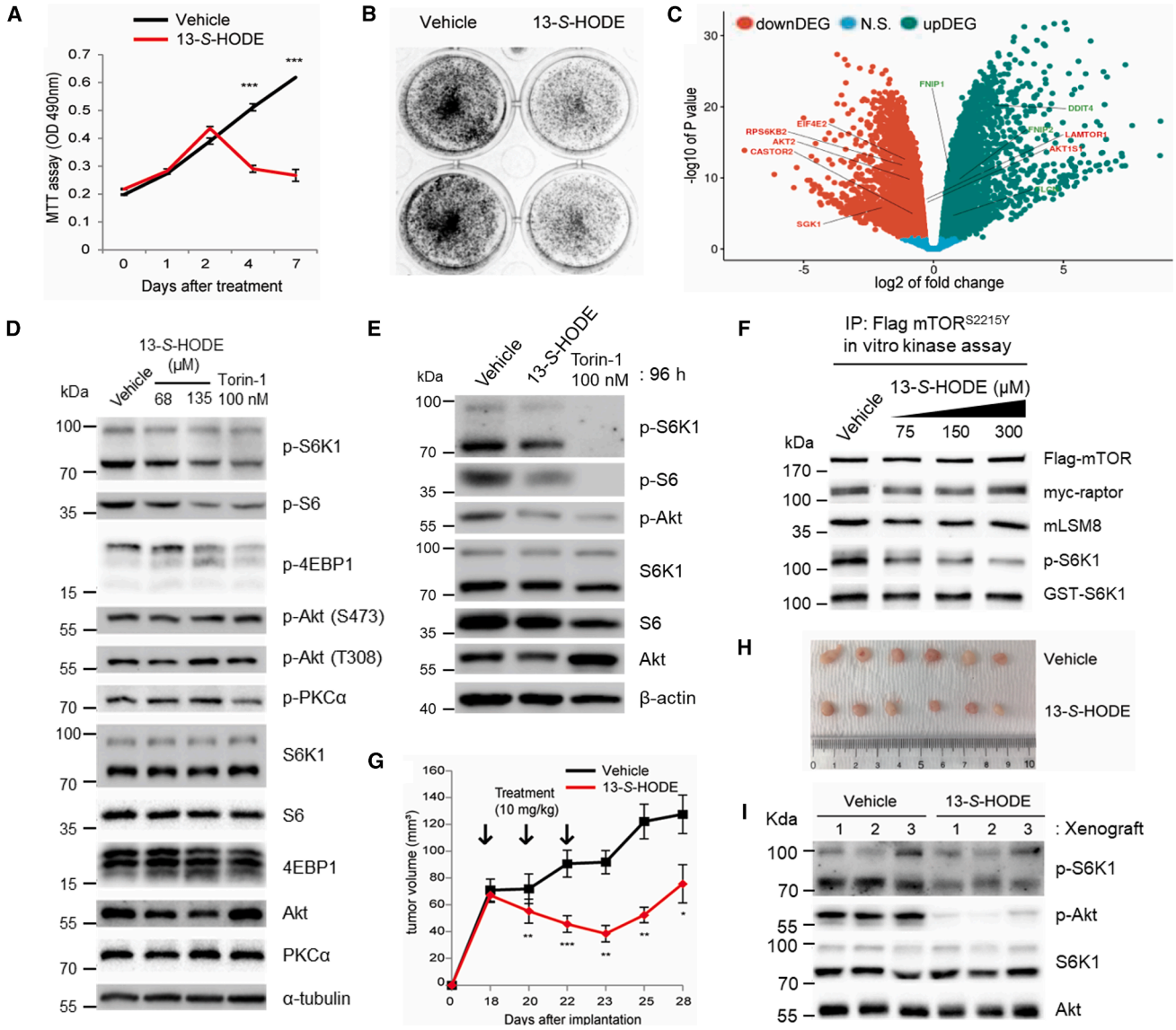

Figure 5. 13-*S*-HODE inhibits mTOR signaling and suppresses the growth of cancer cells with hyperactive *MTOR* mutation

(A and B) Cell viability (A) and colony formation (B) of DMSO vehicle or 135 μM 13-*S*-HODE treated JHUEM7 endometrial cancer cells were measured.

(C) Volcano plot showing significant gene expression changes in response to 135 μM 13-*S*-HODE treatment in JHUEM7 cells. (D) JHUEM7 cells were treated with DMSO vehicle or 13-*S*-HODE for 48 h.

Cell lysates were analyzed by immunoblotting for the levels of the indicated proteins and phosphorylation states.

(E) JHUEM7 cells were treated with DMSO vehicle or 135 μM 13-*S*-HODE for 96 h. Cell lysates were analyzed by immunoblotting for the levels of the indicated proteins and phosphorylation states.

(F) *In vitro* mTORC1 activity of mTOR immunoprecipitates prepared from HEK293T cells expressing mTOR^{S2215Y} was assayed in the presence of 13-*S*-HODE.

(G–I) JHUEM7 cancer cells were inoculated into flanks of nude mice (n = 6 per group) and tumor volumes were measured for 28 days after injection.

DMSO vehicle or 13-*S*-HODE (10 mg/kg) were intratumorally injected three times into xenograft tumors every 2 days (G).

Data are expressed as mean ± SE (*p < 0.05, **p < 0.01, ***p < 0.001, Student's t test.). Representative images of xenograft tumors at the day of sacrifice (H).

Immunoblot analysis of tumor tissues harvested from xenograft (I).

Data are representative of three independent experiments.

mTOR^{C1483Y}, and mTOR^{E1799K}, their kinase activities were dramatically suppressed in the presence of 13-*S*-HODE (Figures 5F, S5F, and S5G). Similarly, inhibition of hyperactive mTOR signaling and cellular growth was also found in 13-*S*-HODE-treated HEC59 endometrial carcinoma cells harboring the mTORC1-activating *MTOR* E1799K mutation (Figures S5H–S5J). These results validate the suppressive effect of 13-*S*-HODE on cancer cells with a hyperactive *MTOR* mutation. Furthermore, the effect of 13-*S*-HODE on tumor growth *in vivo* was examined by injecting JHUEM7 cells subcutaneously into immunocompromised mice and monitoring tumor growth. mTOR signaling activities were markedly suppressed and

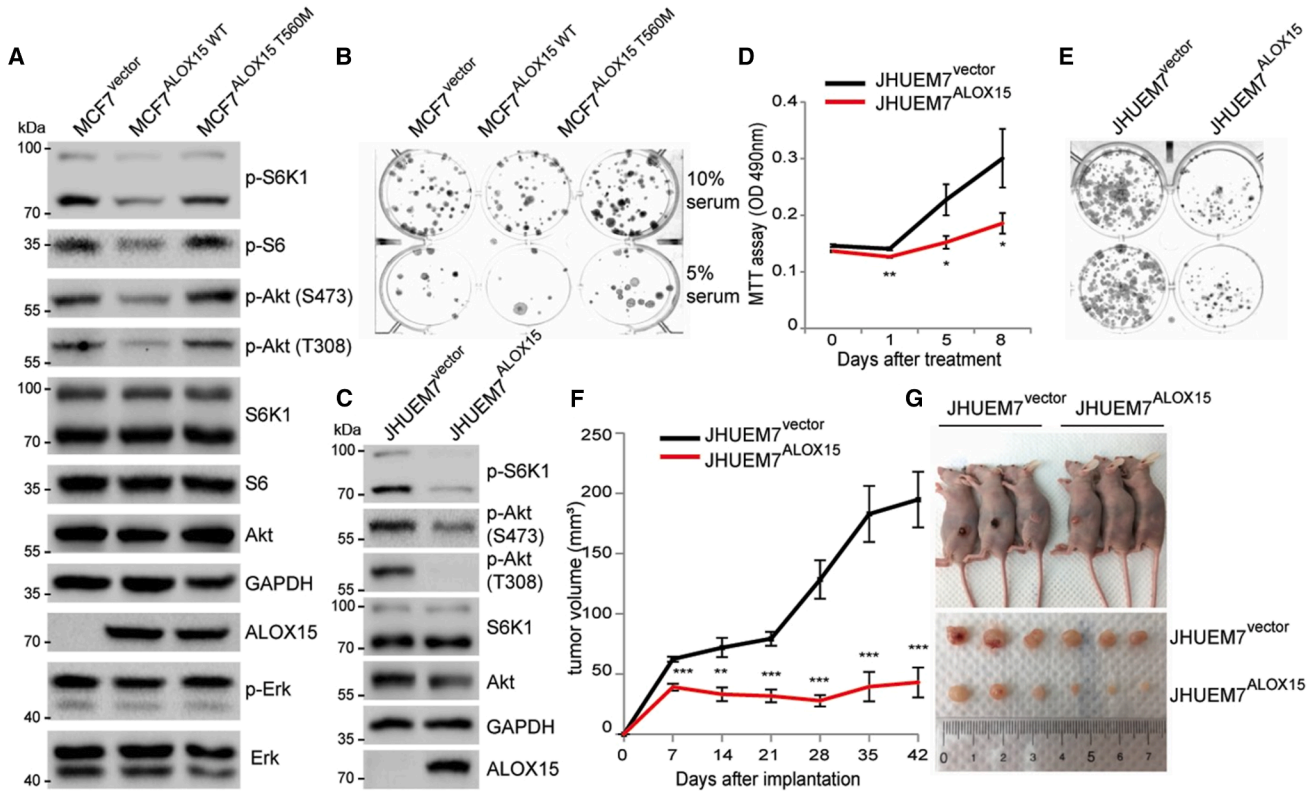

Figure 6. ALOX15 overexpression reduces mTOR signaling and cancer cell growth

(A and B) MCF7 cells with stable overexpression of empty vector, ALOX15-WT, or ALOX15-T560M were generated. Cell lysates were analyzed by immunoblotting for the levels of the indicated proteins and phosphorylation states (A). Colony formation of MCF7 cells in (*A*) was measured (B).

(C–G) JHUEM7 cells with stable overexpression of empty vector or ALOX15-WT were generated. Cell lysates were analyzed by immunoblotting for the levels of the indicated proteins and phosphorylation states (C).

Cell viability (D) and colony formation (E) of JHEUM7 cells were measured. JHUEM7 cells were inoculated into flanks of nude mice (n = 6 per group) and tumor volumes were measured for 42 days after injection (F).

Data are expressed as mean ± SE (*p < 0.05, **p < 0.01, ***p < 0.001, Student's t test.). Representative images of xenograft tumors at the day of sacrifice (G).

growth of the JHUEM7 xenograft was stunted only when 13-*S*-HODE was injected intratumorally (Figures 5G–5I) or intravenously (Figure S5K and S5L), thus confirming 13-*S*-HODE's anti-tumorigenic potentials.

ALOX15 overexpression reduces mTOR signaling and cancer cell growth

To further examine our hypothesis, we tested whether mTOR signaling can be affected by the expression of ALOX15 which is found down-regulated in many cancer cells.[31,32] We first chose MCF7 breast cancer cells with active PI3K signaling pathway. Compared with control cells expressing empty vector (MCF7^{vector}), MCF7 cells stably overexpressing wild-type ALOX15 (MCF7$^{ALOX15\ WT}$) exhibited dramatically reduced phosphorylation of S6K1 T389 and Akt S473 (Figure 6A), indicating inhibition of both mTORC1 and C2. In contrast, no significant decrease in mTOR signaling was observed upon expression of catalytically inactive mutant ALOX15 T560M (MCF7$^{ALOX15\ T560M}$,[38] (Figure 6A), suggesting the role of catalytic action of ALOX15 in the suppression of mTOR in cancer cells. Consistent with these observations, expression of ALOX15-WT, but not ALOX15-T560M, suppressed colony formation of MCF7 cells (Figure 6B).

We also established hyperactive *MTOR*-harboring JHUEM7 cells stably overexpressing ALOX15-WT. Compared to vector-expressing control cells (JHUEM7^{vector}), overexpression of ALOX15 in JHUEM7 cells (JHUEM7^{ALOX15}) led to decreased phosphorylation of both S6K1 T389 and Akt S473 (Figure 6C), followed by reduced growth of cell culture (Figure 6D) and colony formation (Figure 6E) as well as tumor xenograft (Figures 6F and 6G). Collectively, these results clearly support a model in which 13-*S*-HODE is the key determinant of mTOR signaling activity and cell growth in cancer cells.

DISCUSSION

Metabolite-protein interactions are key molecular events in mediating control of the fundamental biological processes between protein-based signaling networks and cellular metabolites.[4,5,7,8] Using an unbiased MS-based screening approach, we discovered 13-*S*-HODE as an mTOR-associated metabolite and identified its unique ability to inhibit the kinase activity of mTOR via directly interacting with its ATP-binding catalytic core. Furthermore, we demonstrated that 13-*S*-HODE supplementation or expression of ALOX15 in cancer cells suppresses

mTOR signaling and attenuates cancer growth at both the cellular and physiological level.

mTOR functions as a signaling hub to integrate metabolic alterations such as amino acid uptake and increased glucose utilization.[10,39] Although information on the roles of amino acid- and glucose-sensing events in the regulation of mTOR signaling has emerged,[11,40,41] our understanding of lipid metabolites in the coordination of mTOR has remained largely elusive. To the best of our knowledge, this is the first description of a molecular mechanism by which mTOR is negatively controlled by directly sensing a lipid metabolite. The range of 13-*S*-HODE actions toward mTOR *in vitro* and in cells was found to be in the higher micromolar level. Similarly, other cellular metabolites have shown to exert their biological effects on their protein targets in the micromolar up to the millimolar level, as exemplified from interactions such as fructose-1,6-bisphosphate with Sos1 (Son of sevenless homolog 1),[42] lactate with NDRG3 (N-myc downstream-regulated gene 3).[43] In our biochemical characterization, we found that 13-*S*-HODE potently targets mTORC1 over mTORC2. Indeed, 48 h incubation of cancer cells with 13-*S*-HODE showed mTORC1 inhibition, but interestingly chronic treatment of 13-*S*-HODE over 96 h led to suppression of both the mTORC1 and C2 signaling pathways. 13-*S*-HODE's action in the dual inhibition of mTORC1 and C2 was validated by robust reductions in both S6K1 and Akt signaling in 13-*S*-HODE–treated tumor xenograft tissues. This finding further highlights the value of 13-*S*-HODE's signaling action because selective or incomplete inhibition of mTORC1 was reported to trigger feedback activation of the PI3K/Akt pathway.[44,45] Thus, further investigation is needed to understand signaling and molecular details underlying 13-*S*-HODE's potent cellular impact on mTORC1/2 inhibition.

The levels of bioactive OXLAMs such as 13-*S*-HODE have been connected to the pathologies of major diseases such as cancer and coronary heart disease.[46,47] Since mammals do not have enzymes to catalyze the *de novo* synthesis of linoleic acid, the intracellular extent to which it can be regulated (through diet, fatty acid transport, or metabolic transformation) needs to be uncovered. For instance, chronic headache and other pain sources can be managed in patients by controlling linoleic acid and its OXLAMs via dietary intervention.[48] Modulation of fatty acid transport in cancer cells has also drawn attention because the control of fatty acid uptake in tumor cells is crucial for the progression of cancer.[49,50] Given that ALOX15 expression is markedly suppressed in many types of cancer, resulting in extremely low intracellular 13-*S*-HODE levels,[28,31,32] achieving relatively high concentrations appears to be crucial for eliciting measurable anti-cancer effects (Figures 4 and 5). Consistent with this notion, our data showed that 13-*S*-HODE suppressed cancer cell proliferation with an EC_{50} of approximately 150 μM (Figure S5A), highlighting the need for pharmacological levels of 13-*S*-HODE to achieve tumor-suppressive activity. Approaches to overcome silenced ALOX15 expression in cancer cells might also provide a way to employ 13-*S*-HODE mediated mTOR control. Thus, further investigations are required to understand fatty acid transporters and metabolic processes related to 13-*S*-HODE in cancer cells. Moreover, a recent study reported a mechanism by which linoleic acid, the precursor of 13-*S*-HODE, can form a complex with fatty acid-binding protein 5 (FABP5), which interacts with raptor to activate mTORC1 in cancer cells including triple-negative breast cancer cells.[51] Future investigations should explore how linoleic acid-triggered mTOR activation[51] and 13-*S*-HODE–mediated mTOR inhibition are finely coordinated in cancer cells.

In summary, we uncovered a previously unknown metabolite-protein interaction that links PUFA metabolism in the case of the oxygenated linoleic acid metabolite, 13-*S*-HODE, to mTOR signaling in cancer. By expanding our classical view of 13-*S*-HODE as an endogenous ligand of the nuclear receptor PPAR,[52] we have established the suppressive action of 13-*S*-HODE on mTOR and cancer cell growth. Our findings suggest that epigenetic silencing of *ALOX15* expression and depletion of 13-*S*-HODE in multiple types of cancers have evolved to avoid its negative action on the mTOR signaling axis, which maintains mTOR activity and supports a favorable cellular milieu for tumor growth. Our study thus provides insight that targeting 13-*S*-HODE lipid metabolism in tumors might be an effective strategy to control mTOR in cancer cells.

13-*S*-HODE, a bioactive oxygenated metabolite of linoleic acid, a polyunsaturated essential fatty acid, directly binds to the catalytic domain of mTOR, thereby inhibiting its kinase activity. Either 13-*S*-HODE treatment or expression of arachidonate 15-lipoxygenase, an enzyme responsible for 13-*S*-HODE production, reduces mTOR and its downstream signaling activities, thus suppressing the growth of cancer cells as well as tumor xenografts. Thus, our data propose 13-*S*-HODE as a tumor suppressive, mTOR-inhibiting cellular metabolite involved in controlling cancer cell growth.

Limitations of the study

While our study identifies 13-*S*-HODE as a novel mTOR-binding metabolite that effectively inhibits mTOR activity and cancer cell growth, several limitations remain to be addressed: First, although our biochemical data demonstrate that 13-*S*-HODE directly suppresses mTOR via occupying the ATP-binding pocket of mTOR, our findings in cells are primarily based on gain-of-function models. Given that 13-*S*-HODE is also a potent inducer of ER stress and ferroptosis-related signaling, we cannot entirely rule out the possibility that these secondary stress responses contribute to an indirect suppression of mTOR. Further studies will be required to dissect the relative contributions of direct biochemical inhibition versus indirect signaling-mediated suppression. Second, the physiological action of the 13-*S*-HODE-mTOR axis remains unknown. Whether the endogenous depletion of ALOX15—and the subsequent reduction in 13-*S*-HODE levels—leads to a reciprocal hyperactivation of mTOR in normal cells is currently unclear. Future research will be needed to determine if this metabolite-protein interaction serves as a fundamental homeostatic regulator of mTOR signaling in diverse biological contexts.

RESOURCE AVAILABILITY

Lead contact

Further information and requests for resources and reagents should be directed to and will be fulfilled by the lead contact, Seyun Kim (seyunkim@kaist.ac.kr).

Materials availability

Materials and reagents generated in this study are available upon reasonable request from the lead contact and may require a completed material transfer agreement.

Data and code availability

- Metabolomics data were deposited on MetaboLights under MTBLS13970. HDX-MS data were deposited on PRIDE under PXD076474. RNA sequencing data were deposited on NCBI Sequence Read Archive (SRA) under PRJNA1432510.
- This article does not report original code.
- Any additional information required to reanalyze the data reported in this article is available from the lead contact upon request.

ACKNOWLEDGMENTS

We are grateful to Dr. Imad Shureiqi (University of Texas MD Anderson Cancer Center) for kindly providing ALOX15 expression plasmid. We also thank the members of the Byun and Kim laboratory, and Seung Min Park for their assistance and advice. We thank Dr. Inhee Mook-Jung for kindly providing U-373 MG cell line (originally from ATCC, Manassas, VA, USA). This work was supported by the grant from the Samsung Science & Technology Foundation (SSTF-BA1401-14 to S.K.), TJ Park Science Fellowship of the POSCO TJ Park Foundation (to S.E.P.), National Research Foundation of Korea (NRF-2020R1I1A1A01073144 to S.J.P.; RS-2024-00337733 and RS-2025-14383304 to M.-Y.K.; RS-2019-NR040070 and RS-2023-00272649 to Y.B.; NRF-2018R1A5A1024261, 2020R1A2C3005765, RS-2023-00278918, RS-2024-00415888, and RS-2025-00519836 to S.K.), KAIST Advanced Institute for Science-X fellowship (to S.J.P.), KAIST Grand Challenge 30 Project N11240024 (to M.-Y.K.), and KAIST Quantum+X Convergence R&D Project (to S.K.). We also thank to Metabolomics core at the Convergence Medicine Research Center, Asan Medical Center for support and instrumentation.

AUTHOR CONTRIBUTIONS

S.J.P., Y.B., and Seyun Kim conceived the work. S.J.P., Sera Kim, H.K., J.C, J.K.K., I.J., S.L., Y.R.K., M.S., A.-Y.Y., B.L., H.L., S.E.P., S.L., B.B.P., Y.K., J.L., and D.D. performed the experiments. S.J.P., Sera Kim, H.K., B.L., B.-C.O., D.D., P.L.W., M.-Y.K., Y.B., and Seyun Kim designed the experiments and analyzed the data. S.J.P., Sera Kim, H.K., D.D., Y.B., and Seyun Kim wrote the manuscript.

DECLARATION OF INTERESTS

The authors declare no competing interests.

STAR★METHODS

Detailed methods are provided in the online version of this paper and include the following:

SUPPLEMENTAL INFORMATION

Supplemental information can be found online at https://doi.org/10.1016/j.chembiol.2026.04.004.

Received: December 15, 2025
Revised: February 11, 2026
Accepted: April 9, 2026
Published: April 30, 2026

REFERENCES

1. Efeyan, A., Comb, W.C., and Sabatini, D.M. (2015). Nutrient-sensing mechanisms and pathways. Nature *517*, 302–310. https://doi.org/10.1038/nature14190.
2. Milanesi, R., Coccetti, P., and Tripodi, F. (2020). The Regulatory Role of Key Metabolites in the Control of Cell Signaling. Biomol *10*, 862. https://doi.org/10.3390/biom10060862.
3. Wang, Y.-P., and Lei, Q.-Y. (2018). Metabolite sensing and signaling in cell metabolism. Signal Transduct. Targeted Ther. *3*, 30. https://doi.org/10.1038/s41392-018-0024-7.
4. Li, X., Gianoulis, T.A., Yip, K.Y., Gerstein, M., and Snyder, M. (2010). Extensive In Vivo Metabolite-Protein Interactions Revealed by Large-Scale Systematic Analyses. Cell *143*, 639–650. https://doi.org/10.1016/j.cell.2010.09.048.
5. Li, X., and Snyder, M. (2011). Metabolites as global regulators: A new view of protein regulation. Bioessays *33*, 485–489. https://doi.org/10.1002/bies.201100026.
6. Schreiber, S.L. (2005). Small molecules: the missing link in the central dogma. Nat. Chem. Biol. *1*, 64–66. https://doi.org/10.1038/nchembio0705-64.
7. McFedries, A., Schwaid, A., and Saghatelian, A. (2013). Methods for the Elucidation of Protein-Small Molecule Interactions. Chem. Biol. *20*, 667–673. https://doi.org/10.1016/j.chembiol.2013.04.008.
8. Tagore, R., Thomas, H.R., Homan, E.A., Munawar, A., and Saghatelian, A. (2008). A Global Metabolite Profiling Approach to Identify Protein−Metabolite Interactions. J. Am. Chem. Soc. *130*, 14111–14113. https://doi.org/10.1021/ja806463c.
9. Ma, X.M., and Blenis, J. (2009). Molecular mechanisms of mTOR-mediated translational control. Nat. Rev. Mol. Cell Biol. *10*, 307–318. https://doi.org/10.1038/nrm2672.
10. Saxton, R.A., and Sabatini, D.M. (2017). mTOR Signaling in Growth, Metabolism, and Disease. Cell *168*, 960–976. https://doi.org/10.1016/j.cell.2017.02.004.
11. Shimobayashi, M., and Hall, M.N. (2014). Making new contacts: the mTOR network in metabolism and signalling crosstalk. Nat. Rev. Mol. Cell Biol. *15*, 155–162. https://doi.org/10.1038/nrm3757.
12. Kim, D.-H., Sarbassov, D.D., Ali, S.M., King, J.E., Latek, R.R., Erdjument-Bromage, H., Tempst, P., and Sabatini, D.M. (2002). mTOR Interacts with Raptor to Form a Nutrient-Sensitive Complex that Signals to the Cell

Growth Machinery. Cell *110*, 163–175. https://doi.org/10.1016/S0092-8674(02)00808-5.

13. Sarbassov, D.D., Ali, S.M., Kim, D.H., Guertin, D.A., Latek, R.R., Erdjument-Bromage, H., Tempst, P., and Sabatini, D.M. (2004). Rictor, a novel binding partner of mTOR, defines a rapamycin-insensitive and raptor-independent pathway that regulates the cytoskeleton. Curr. Biol. *14*, 1296–1302. https://doi.org/10.1016/j.cub.2004.06.054.
14. Sarbassov, D.D., Guertin, D.A., Ali, S.M., and Sabatini, D.M. (2005). Phosphorylation and Regulation of Akt/PKB by the Rictor-mTOR Complex. Science *307*, 1098–1101. https://doi.org/10.1126/science.1106148.
15. Guertin, D.A., and Sabatini, D.M. (2007). Defining the Role of mTOR in Cancer. Cancer Cell *12*, 9–22. https://doi.org/10.1016/j.ccr.2007.05.008.
16. Mossmann, D., Park, S., and Hall, M.N. (2018). mTOR signalling and cellular metabolism are mutual determinants in cancer. Nat. Rev. Cancer *18*, 744–757. https://doi.org/10.1038/s41568-018-0074-8.
17. Cornu, M., Albert, V., and Hall, M.N. (2013). mTOR in aging, metabolism, and cancer. Curr. Opin. Genet. Dev. *23*, 53–62. https://doi.org/10.1016/j.gde.2012.12.005.
18. Menon, S., and Manning, B.D. (2008). Common corruption of the mTOR signaling network in human tumors. Oncogene *27 Suppl 2*, S43–S51. https://doi.org/10.1038/onc.2009.352.
19. Zhou, H., and Huang, S. (2011). Role of mTOR signaling in tumor cell motility, invasion and metastasis. Curr. Protein Pept. Sci. *12*, 30–42. https://doi.org/10.2174/138920311795659407.
20. Hara, K., Maruki, Y., Long, X., Yoshino, K.-I., Oshiro, N., Hidayat, S., Tokunaga, C., Avruch, J., and Yonezawa, K. (2002). Raptor, a Binding Partner of Target of Rapamycin (TOR), Mediates TOR Action. Cell *110*, 177–189. https://doi.org/10.1016/S0092-8674(02)00833-4.
21. Peterson, T.R., Laplante, M., Thoreen, C.C., Sancak, Y., Kang, S.A., Kuehl, W.M., Gray, N.S., and Sabatini, D.M. (2009). DEPTOR Is an mTOR Inhibitor Frequently Overexpressed in Multiple Myeloma Cells and Required for Their Survival. Cell *137*, 873–886. https://doi.org/10.1016/j.cell.2009.03.046.
22. Sancak, Y., Thoreen, C.C., Peterson, T.R., Lindquist, R.A., Kang, S.A., Spooner, E., Carr, S.A., and Sabatini, D.M. (2007). PRAS40 Is an Insulin-Regulated Inhibitor of the mTORC1 Protein Kinase. Mol. Cell *25*, 903–915. https://doi.org/10.1016/j.molcel.2007.03.003.
23. Fang, Y., Vilella-Bach, M., Bachmann, R., Flanigan, A., and Chen, J. (2001). Phosphatidic Acid-Mediated Mitogenic Activation of mTOR Signaling. Science *294*, 1942–1945. https://doi.org/10.1126/science.1066015.
24. Spiteller, G. (1998). Linoleic acid peroxidation—the dominant lipid peroxidation process in low density lipoprotein—and its relationship to chronic diseases. Chem. Phys. Lipids *95*, 105–162. https://doi.org/10.1016/S0009-3084(98)00091-7.
25. Il Lee, S., Zuo, X., and Shureiqi, I. (2011). 15-Lipoxygenase-1 as a tumor suppressor gene in colon cancer: is the verdict in? Cancer Metastasis Rev. *30*, 481–491. https://doi.org/10.1007/s10555-011-9321-0.
26. Shureiqi, I., Jiang, W., Zuo, X., Wu, Y., Stimmel, J.B., Leesnitzer, L.M., Morris, J.S., Fan, H.-Z., Fischer, S.M., and Lippman, S.M. (2003). The 15-lipoxygenase-1 product 13-S-hydroxyoctadecadienoic acid down-regulates PPAR-δ to induce apoptosis in colorectal cancer cells. Proc. Natl. Acad. Sci. USA *100*, 9968–9973. https://doi.org/10.1073/pnas.1631086100.
27. Shureiqi, I., Wu, Y., Chen, D., Yang, X.L., Guan, B., Morris, J.S., Yang, P., Newman, R.A., Broaddus, R., Hamilton, S.R., et al. (2005). The Critical Role of 15-Lipoxygenase-1 in Colorectal Epithelial Cell Terminal Differentiation and Tumorigenesis. Cancer Res. *65*, 11486–11492. https://doi.org/10.1158/0008-5472.CAN-05-2180.
28. Tian, R., Zuo, X., Jaoude, J., Mao, F., Colby, J., and Shureiqi, I. (2017). ALOX15 as a suppressor of inflammation and cancer: Lost in the link. Prostag. Other Lipid Mediat. *132*, 77–83. https://doi.org/10.1016/j.prostaglandins.2017.01.002.
29. Yang, H., Rudge, D.G., Koos, J.D., Vaidialingam, B., Yang, H.J., and Pavletich, N.P. (2013). mTOR kinase structure, mechanism and regulation. Nature *497*, 217–223. https://doi.org/10.1038/nature12122.
30. Grabiner, B.C., Nardi, V., Birsoy, K., Possemato, R., Shen, K., Sinha, S., Jordan, A., Beck, A.H., and Sabatini, D.M. (2014). A Diverse Array of Cancer-Associated MTOR Mutations Are Hyperactivating and Can Predict Rapamycin Sensitivity. Cancer Discov. *4*, 554–563. https://doi.org/10.1158/2159-8290.CD-13-0929.
31. Moussalli, M.J., Wu, Y., Zuo, X., Yang, X.L., Wistuba, I.I., Raso, M.G., Morris, J.S., Bowser, J.L., Minna, J.D., Lotan, R., and Shureiqi, I. (2011). Mechanistic Contribution of Ubiquitous 15-Lipoxygenase-1 Expression Loss in Cancer Cells to Terminal Cell Differentiation Evasion. Cancer Prev. Res. *4*, 1961–1972. https://doi.org/10.1158/1940-6207.CAPR-10-0280.
32. Shureiqi, I., Wojno, K.J., Poore, J.A., Reddy, R.G., Moussalli, M.J., Spindler, S.A., Greenson, J.K., Normolle, D., Hasan, A.A., Lawrence, T.S., and Brenner, D.E. (1999). Decreased 13-S-hydroxyoctadecadienoic acid levels and 15-lipoxygenase-1 expression in human colon cancers. Carcinogenesis *20*, 1985–1995. https://doi.org/10.1093/carcin/20.10.1985.
33. Aylett, C.H.S., Sauer, E., Imseng, S., Boehringer, D., Hall, M.N., Ban, N., and Maier, T. (2016). Architecture of human mTOR complex 1. Science *351*, 48–52. https://doi.org/10.1126/science.aaa3870.
34. Chen, X., Liu, M., Tian, Y., Li, J., Qi, Y., Zhao, D., Wu, Z., Huang, M., Wong, C.C.L., Wang, H.-W., et al. (2018). Cryo-EM structure of human mTOR complex 2. Cell Res. *28*, 518–528. https://doi.org/10.1038/s41422-018-0029-3.
35. Stuttfeld, E., Aylett, C.H., Imseng, S., Boehringer, D., Scaiola, A., Sauer, E., Hall, M.N., Maier, T., and Ban, N. (2018). Architecture of the human mTORC2 core complex. eLife *7*, e33101. https://doi.org/10.7554/eLife.33101.
36. Tafur, L., Kefauver, J., and Loewith, R. (2020). Structural Insights into TOR Signaling. Genes *11*, 885. https://doi.org/10.3390/genes11080885.
37. Yang, H., Wang, J., Liu, M., Chen, X., Huang, M., Tan, D., Dong, M.Q., Wong, C.C.L., Wang, J., Xu, Y., and Wang, H.W. (2016). 4.4 Å Resolution Cryo-EM structure of human mTOR Complex 1. Protein Cell *7*, 878–887. https://doi.org/10.1007/s13238-016-0346-6.
38. Schurmann, K., Anton, M., Ivanov, I., Richter, C., Kuhn, H., and Walther, M. (2011). Molecular basis for the reduced catalytic activity of the naturally occurring T560M mutant of human 12/15-lipoxygenase that has been implicated in coronary artery disease. J. Biol. Chem. *286*, 23920–23927. https://doi.org/10.1074/jbc.M110.211821.
39. Kim, J., and Guan, K.-L. (2019). mTOR as a central hub of nutrient signalling and cell growth. Nat. Cell Biol. *21*, 63–71. https://doi.org/10.1038/s41556-018-0205-1.
40. Laplante, M., and Sabatini, D.M. (2012). mTOR Signaling in Growth Control and Disease. Cell *149*, 274–293. https://doi.org/10.1016/j.cell.2012.03.017.
41. Orozco, J.M., Krawczyk, P.A., Scaria, S.M., Cangelosi, A.L., Chan, S.H., Kunchok, T., Lewis, C.A., and Sabatini, D.M. (2020). Dihydroxyacetone phosphate signals glucose availability to mTORC1. Nat. Metab. *2*, 893–901. https://doi.org/10.1038/s42255-020-0250-5.
42. Peeters, K., Van Leemputte, F., Fischer, B., Bonini, B.M., Quezada, H., Tsytlonok, M., Haesen, D., Vanthienen, W., Bernardes, N., Gonzalez-Blas, C.B., et al. (2017). Fructose-1,6-bisphosphate couples glycolytic flux to activation of Ras. Nat. Commun. *8*, 922. https://doi.org/10.1038/s41467-017-01019-z.
43. Lee, D.C., Sohn, H.A., Park, Z.-Y., Oh, S., Kang, Y.K., Lee, K.-m., Kang, M., Jang, Y.J., Yang, S.-J., Hong, Y.K., et al. (2015). A Lactate-Induced Response to Hypoxia. Cell *161*, 595–609. https://doi.org/10.1016/j.cell.2015.03.011.
44. Benjamin, D., Colombi, M., Moroni, C., and Hall, M.N. (2011). Rapamycin passes the torch: a new generation of mTOR inhibitors. Nat. Rev. Drug Discov. *10*, 868–880. https://doi.org/10.1038/nrd3531.

45. O'Reilly, K.E., Rojo, F., She, Q.-B., Solit, D., Mills, G.B., Smith, D., Lane, H., Hofmann, F., Hicklin, D.J., Ludwig, D.L., et al. (2006). mTOR Inhibition Induces Upstream Receptor Tyrosine Kinase Signaling and Activates Akt. Cancer Res. *66*, 1500–1508. https://doi.org/10.1158/0008-5472.can-05-2925.

46. Das, U.N. (2006). Essential fatty acids: biochemistry, physiology and pathology. Biotechnol. J. *1*, 420–439. https://doi.org/10.1002/biot.200600012.

47. Vangaveti, V.N., Jansen, H., Kennedy, R.L., and Malabu, U.H. (2016). Hydroxyoctadecadienoic acids: Oxidised derivatives of linoleic acid and their role in inflammation associated with metabolic syndrome and cancer. Eur. J. Pharmacol. *785*, 70–76. https://doi.org/10.1016/j.ejphar.2015.03.096.

48. Ramsden, C.E., Faurot, K.R., Zamora, D., Palsson, O.S., MacIntosh, B.A., Gaylord, S., Taha, A.Y., Rapoport, S.I., Hibbeln, J.R., Davis, J.M., and Mann, J.D. (2015). Targeted alterations in dietary n-3 and n-6 fatty acids improve life functioning and reduce psychological distress among patients with chronic headache: a secondary analysis of a randomized trial. Pain *156*, 587–596. https://doi.org/10.1097/01.j.pain.0000460348.84965.47.

49. Corn, K.C., Windham, M.A., and Rafat, M. (2020). Lipids in the tumor microenvironment: From cancer progression to treatment. Prog. Lipid Res. *80*, 101055. https://doi.org/10.1016/j.plipres.2020.101055.

50. Watt, M.J., Clark, A.K., Selth, L.A., Haynes, V.R., Lister, N., Rebello, R., Porter, L.H., Niranjan, B., Whitby, S.T., Lo, J., et al. (2019). Suppressing fatty acid uptake has therapeutic effects in preclinical models of prostate cancer. Sci. Transl. Med. *11*, eaau5758. https://doi.org/10.1126/scitranslmed.aau5758.

51. Koundouros, N., Nagiec, M.J., Bullen, N., Noch, E.K., Burgos-Barragan, G., Li, Z., He, L., Cho, S., Parang, B., Leone, D., et al. (2025). Direct sensing of dietary ω-6 linoleic acid through FABP5-mTORC1 signaling. Science *387*, eadm9805. https://doi.org/10.1126/science.adm9805.

52. Itoh, T., Fairall, L., Amin, K., Inaba, Y., Szanto, A., Balint, B.L., Nagy, L., Yamamoto, K., and Schwabe, J.W.R. (2008). Structural basis for the activation of PPARγ by oxidized fatty acids. Nat. Struct. Mol. Biol. *15*, 924–931. https://doi.org/10.1038/nsmb.1474.

53. Yoon, M.S., Sun, Y., Arauz, E., Jiang, Y., and Chen, J. (2011). Phosphatidic acid activates mammalian target of rapamycin complex 1 (mTORC1) kinase by displacing FK506 binding protein 38 (FKBP38) and exerting an allosteric effect. J. Biol. Chem. *286*, 29568–29574. https://doi.org/10.1074/jbc.M111.262816.

54. Vilella-Bach, M., Nuzzi, P., Fang, Y., and Chen, J. (1999). The FKBP12-rapamycin-binding domain is required for FKBP12-rapamycin-associated protein kinase activity and G1 progression. J. Biol. Chem. *274*, 4266–4272. https://doi.org/10.1074/jbc.274.7.4266.

55. Houde, D., Berkowitz, S.A., and Engen, J.R. (2011). The Utility of Hydrogen/Deuterium Exchange Mass Spectrometry in Biopharmaceutical Comparability Studies. J. Pharmacol. Sci. *100*, 2071–2086. https://doi.org/10.1002/jps.22432.

56. Huynh, K., and Partch, C.L. (2015). Analysis of Protein Stability and Ligand Interactions by Thermal Shift Assay. Curr. Protoc. Protein Sci. *79*, 28.9.1–28.9.14. https://doi.org/10.1002/0471140864.ps2809s79.

57. Shin, M., and Byun, Y. (2024). Stereoselective Syntheses of Polyunsaturated Fatty Acids, 13-(S)-HODE and 15-(S)-HETE. J. Org. Chem. *89*, 11293–11303. https://doi.org/10.1021/acs.joc.4c00983.

STAR★METHODS

KEY RESOURCES TABLE

REAGENT or RESOURCE	SOURCE	IDENTIFIER
Antibodies		
mTOR polyclonal rabbit antibody	Cell Signaling Technology	Cat#2972 S; RRID: AB_330978
Raptor polyclonal rabbit Ab	Bethyl Laboratories	Cat#A300-553 A; RRID:AB_2130793
Rictor polyclonal rabbit Ab	Bethyl Laboratories	Cat#A300-459 A; RRID:AB_2179967
Phospho-p70 S6 Kinase (Thr389) polyclonal rabbit Ab	Cell Signaling Technology	Cat#9205 S; RRID:AB_330944
p70 S6 Kinase polyclonal rabbit Ab	Cell Signaling Technology	Cat#9202 S; RRID:AB_331676
Phospho-AKT (Ser473) monoclonal rabbit Ab	Cell Signaling Technology	Cat#4058 S; RRID:AB_331168
Phospho-AKT (T308) monoclonal rabbit Ab	Cell Signaling Technology	Cat#13038 S; RRID:AB_2629447
AKT (pan) monoclonal rabbit Ab	Cell Signaling Technology	Cat#4691 S; RRID:AB_915783
Phospho-S6 Ribosomal Protein (Ser240/244) (D68F8) XP® monoclonal rabbit Ab	Cell Signaling Technology	Cat#5364 S; RRID:AB_10694233
S6 Ribosomal Protein (5G10) monoclonal rabbit Ab	Cell Signaling Technology	Cat#2217 S; RRID:AB_331355
GBL monoclonal rabbit Ab	Cell Signaling Technology	Cat#3274 S; RRID:AB_823685
Phospho-4E-BP1 (Thr37/46) polyclonal rabbit Ab	Cell Signaling Technology	Cat#9459 S; RRID:AB_330985
4 E-BP1 (53H11) polyclonal rabbit Ab	Cell Signaling Technology	Cat#9644 S; RRID:AB_2097841
PKCα (D7E6 E) monoclonal rabbit Ab	Cell Signaling Technology	Cat#59754 S; RRID:AB_2799573
Phospho-PKCα/β II (Thr638/641) polyclonal rabbit Ab	Cell Signaling Technology	Cat#9375 S; RRID:AB_2284224
Phospho-p44/42 MAPK (Erk1/2) (Thr202/Tyr204) polyclonal rabbit Ab	Cell Signaling Technology	Cat#9101 S; RRID:AB_331646
p44/42 MAPK (Erk1/2) polyclonal mouse Ab	Cell Signaling Technology	Cat#9102 S; RRID:AB_330744
ALOX15 monoclonal rabbit Ab	Biorbyt	Cat#orb247636
β-actin monoclonal rabbit Ab	Cell Signaling Technology	Cat#4970 S; RRID:AB_2223172
GAPDH monoclonal mouse Ab	Santa Cruz	Cat#sc-47724; RRID:AB_627678
GST-Tag polyclonal rabbit Ab	Cell Signaling Technology	Cat#2622 S; RRID:AB_331670
Myc-Tag (71D10) monoclonal rabbit Ab	Cell Signaling Technology	Cat#2278 T; RRID:AB_490778
FLAG monoclonal rabbit Ab	Invitrogen	Cat#F1804-200UG; RRID:AB_262044
Anti-rabbit IgG, HRP-linked Antibody	Cell Signaling Technology	Cat#7074 S; RRID:AB_2099233
Anti-mouse IgG, HRP-linked Antibody	Cell Signaling Technology	Cat#7076 S; RRID:AB_330924
Bacterial and virus strains		
DH5α Competent Cells	This paper	N/A
Stbl3 Competent Cells	This paper	N/A
Chemicals, peptides, and recombinant proteins		
(*E*)-non-3-en-1-ol	Enamine	EN300-22935798-10G
Tetrahydrofuran (THF), 99.5%	Thermo Fisher Scientific	348450010-1 L
Sodium hydride (NaH, 60% dispersion in mineral oil)	Sigma-Aldrich	452912-100G
4-Methoxybenzyl Chloride (PMBCl, stabilized with Amylene)	TCI	M0676-25ML
Tetrabutylammonium bromide (TBAB)	TCI	T0054-100G
Ammonium chloride, 99.0% (NH_4Cl)	Samchun Chemical	A0711-1KG
Magnesium sulfate, anhydrous, 99.5% ($MgSO_4$)	Samchun Chemical	M0146-1KG

(*Continued on next page*)

Continued

REAGENT or RESOURCE	SOURCE	IDENTIFIER
Hexane (95.0%)	Samchun Chemical	H0114-18 L
Potassium ferricyanide, $K_3[Fe(CN)_6]$ (ACS reagent, ≥99.0%)	Sigma-Aldrich	244023-500G
K_2CO_3 (ACS reagent, ≥99.0%)	Sigma-Aldrich	209619-1KG
$(DHQ)_2PHAL$ (≥95.0%)	Sigma-Aldrich	392723-500MG
$(DHQD)_2PHAL$ (≥95.0%)	Sigma-Aldrich	392731-1G
tert-BuOH (ACS reagent, ≥99.0%)	Sigma-Aldrich	360538-1 L
Potassium osmate (VI) dihydrate ($K_2OsO_4 \cdot 2H_2O$)	Thermo Fisher Scientific	197665000-500MG
Methanesulfonamide (≥97.0%)	Sigma-Aldrich	64275-10G
Na_2SO_3 (95%)	Samchun Chemical	S1053-1KG
Dimethyl carbonate	TCI	C0053-100ML
Dichloromethane (DCM, anhydrous, ≥99.8%, contains 40–150 ppm amylene as stabilizer)	Sigma-Aldrich	270997-1 L
2,3-Dichloro-5,6-dicyano-*p*-benzoquinone (DDQ, 98%)	Sigma-Aldrich	D60400-10G
60 Silica gel (230–450 mesh)	Thermo Fisher Chemical	L14003.0 B-1KG
2-Iodoxybenzoic acid (IBX, 45% w/w with stabilizer)	Sigma-Aldrich	661384-10G
Triphenylphosphine (>95.0%)	TCI	T0519-100G
9-Bromononanoic acid (>97.0%)	TCI	B2323-5G
Toluene (ACS reagent, ≥99.5%)	Sigma-Aldrich	179418-1 L
Diethyl ether (≥99.0%, anhydrous, ACS reagent, contains BHT as inhibitor)	Sigma-Aldrich	346136-1 L
N,N′-Dimethylpropyleneurea (DMPU, >98.0%)	TCI	D2014-100G
1.5 M lithium bis(trimethylsilyl) amide (LiHMDS) solution in THF	Sigma-Aldrich	766917-100ML
Methyl *tert*-Butyl Ether (HPLC), Fisher Chemical	Thermo Fisher Scientific	E127-4 (4 L)
Hexanes (HPLC), Fisher Chemical	Thermo Fisher Scientific	H302-4 (4 L)
HCl (37%, ACS reagent)	Sigma-Aldrich	258148-100ML
13(S)-HODE	Cayman	Cat#38610
13(S)-HODE-biotin	Cayman	Cat#38612
Linoleic Acid-Water Soluble	Sigma-Aldrich	Cat#L5900-10MG
Biotin-linoleic acid	Larodan	Cat#39-1802-39
15(S)HETE	Cayman	Cat#34720
15(S)-HETE-biotin	Cayman	Cat#34722
Biotin	Sigma-Aldrich	Cat#B4639-1G
Torin-1	MCE	Cat#MCE-HY-13003-5MG
mTOR (1362-end), active, 10 μg	Sigma-Aldrich	Cat#14-770-M
AKT1, Inactive, His-tag Recombinant	BPS	Cat#40000-1
Adenosine 5′-triphosphate disodium salt hydrate	Sigma-Aldrich	Cat#A7699-1G
Rabbit TrueBlot®: Anti-Rabbit IgG HRP	Rockland	Cat#18-8816-31
Pierce™ Streptavidin Magnetic Beads	Sigma-Aldrich	Cat#88816
ANTI-FLAG® M2 Affinity Gel	Millipore	Cat#A2220-5ML
Glutathione Resin	Genescript	Cat#L00206
jetPRIME® transfection reagent	Polyplus transfection	Cat#114-15
CHAPS hydrate	Sigma-Aldrich	Cat#C3023-5 g
Nonidet P40 Substitute	Georgiachem	Cat#9036-19-5

(*Continued on next page*)

Continued

REAGENT or RESOURCE	SOURCE	IDENTIFIER
Sodium Chloride	LPS solution	Cat#NACL05
1 M HEPES	Welgene	Cat#BB01240701
UltraPure™ 0.5 M EDTA, pH8.0	Invitrogen	Cat#2323123
Protease inhibitor cocktail (Complete)	Roche	Cat#11836145001
Sodium pyrophosphate tetrabasic	Sigma-Aldrich	Cat#P8010-500G
Sodium Fluoride	Sigma-Aldrich	Cat#201154-100G
Magnesium chloride hexahydrate	Sigma-Aldrich	Cat#M7304-100G
Potassium acetate	Sigma-Aldrich	Cat#P1190-500G
Potassium chloride	Sigma-Aldrich	Cat#529552-250GM
Glycerol	Sigma-Aldrich	Cat#G5516-500ML
Dimethyl sulfoxide	Sigma-Aldrich	Cat#D4540-100ML
Deuterium oxide	Sigma-Aldrich	Cat#293040-25G
0.5 M EGTA, pH 8.0	Biosolution	Cat#BE004-1
Brij® L23	Sigma-Aldrich	Cat#P1254-500G
Sodium orthovanadate	Sigma-Aldrich	Cat#567540-5GM
DL-Dithiothreitol (DTT)	LPS solution	Cat#DTT025
Ethyl acetate (ACS reagent, ≥99.5%)	Sigma-Aldrich	Cat#319902-1 L
Crystal Violet	Sigma-Aldrich	Cat#C0775-25G
3-(4,5-dimethylthiazol-2-yl)-2,5-diphenyl tetrazolium bromide (MTT) formazan	Sigma-Aldrich	Cat#88417-1G
SYPRO® Orange Protein Gel Stain	Sigma-Aldrich	Cat#S5692-50UL
30% Acrylamide/Bis Solution, 29:1	Bio-Rad	Cat#1610156
Ammonium persulfate	Sigma-Aldrich	Cat#A3678-25G
N,N,N′,N′-Tetramethylethylenediamine	Sigma-Aldrich	Cat#T9281-100ML
Bio-Rad Protein Assay Dye Reagent Concentrate	Bio-Rad	Cat#5000006
PageRuler Prestained Protein Ladder	Thermo fisher	Cat#26616
Spectra™ Multicolor High Range Protein Ladder	Thermo fisher	Cat#26625
SuSignal™ West Femto Maximum Sensitivity Substrate	Thermo fisher	Cat#34095
Immobilon Forte Western HRP substrate	Millipore	Cat#WBLUF0500
Penicillin-Streptomycin (10,000 U/mL)	Gibco	Cat#15140122
Trypsin-EDTA (500mL)	Welgene	Cat#LS-015-10
MEM Non-Essential Amino Acids Solution (100×)	Gibco	Cat#11140050
Bovine serum albumin (BSA)	Sigma-Aldrich	Cat#A9647-500 g
Ampicillin Sodium Salt	LPS solution	Cat#AMP10
LB Broth (High Salt)	LPS solution	Cat#LB-05
Acetonitrile (≥99.5%, ACS reagent)	Sigma-aldrich	Cat#360457-1 L
Acetonitrile 99.5%, Extra Pure	DAEJUNG	Cat#1012-4404
HPLC Water	DAEJUNG	Cat#8585-2305
Critical commercial assays		
EZ-cytox WST-1	Dozen	EZ-3000
Experimental models: Cell lines		
Human: JHEUM7	RIKEN	ID#RCB1677
Human: HEK293	American Type Culture Collection	ID#CRL-1573™
Human: HEK293T	American Type Culture Collection	ID#CRL-3216
Human: HeLa	American Type Culture Collection	N/A
Human: MCF10A	In-house	N/A
Human: MDA-MB-468	In-house	N/A

(*Continued on next page*)

Continued

REAGENT or RESOURCE	SOURCE	IDENTIFIER
Human: U373-MG	In-house	N/A
Human: HT-29	In-house	N/A
Human: HEC59	JCRB Cell Bank	ID#JCRB1120
Human: NCM460D	INCELL	ID#NCM460D
Human: SW480	In-house	N/A
Experimental models: Organisms/strains		
Mouse: CAnN.Cg-*Foxn1*^{nu}/Crl, Female	This paper	N/A
Oligonucleotides		
Primers for GST-S6K1 (amino acids 332–421) Fw: CGCGGATCCTAATTTGCCTC CCTACCTCACA, Rv: CCGGAATTCAGAG TTGAGTCATCGGGGCT	J Chen et al.[53]	N/A
Recombinant DNA		
pGEX-4T3-GST-S6K1 (amino acids 332–421)	J Chen et al.[53]	N/A
pCDH-MCS-T2A-copGFP-MSCV	System Biosciences	Cat#CD523A-1
pcDNA3-Flag mTOR^{WT}	Gift from Jie Chen[54]	Addgene plasmid #26603
myc-Raptor	Gift from David Sabatini[13]	Addgene plasmid #1859
myc-Rictor corrected	Gift from David Sabatini[13]	Addgene plasmid #11367
Deposited data		
Metabolomics data	MetaboLights	MTBLS13970
RNA-sequencing data	SRA	PRJNA1432510
HDX-MS data	PRIDE	Project accession: PXD076474
Software and algorithms		
ChemBioDraw (ver. 11.0.1)	Revvity Signals Software	https://revvitysignals.com/products/research/chemdraw
Chem3D Pro (ver. 11.0.1)	CambridgeSoft Corp	https://www.cambridgesoftware.com/
BIOVIA Discovery Studio 3.0	Dassault Systèmes	RRID:SCR_014695; https://discover.3ds.com/discovery-studio-visualizer-download
PyMOL software	Schrodinger	RRID:SCR_000305; https://www.pymol.org/
ImageJ	National Institutes of Health	RRID: SCR_003070; https://imagej.net/ij/download.html
GraphPad Prism (version 8.0)	GraphPad software	RRID: SCR_002798; https://www.graphpad.com/
Other		
Dulbecco's Modified Eagle's Medium (DMEM)	Welgene	Cat#LM001-05
DMEM Hams F12 Medium	Welgene	Cat#LM002-04
Roswell Park Memorial Institute 1640 (RPMI1640)	Welgene	Cat#LM 011-01
Minimum Essential Medium (MEM)	Welgene	Cat#LM 007-54
Dulbecco's Phosphate Buffered Saline (DPBS)	Welgene	Cat#LB001-02
Fetal bovine serum (FBS)	Atlas	Cat#FP-0500-A
UPLC C18 column	Avantar	Cat# EXL-171-1002U
250 mm × 4.6 mm, 5 μm, Daicel Chiralpak-IG (chiral HPLC column)	DAICEL CORPORATION	Lot No. IG00CE-UJ024
250 × 4.6 mm, Nacalai Cosmosil Cholester packed column	Nacalai	05977–51

EXPERIMENTAL MODEL AND STUDY PARTICIPANT DETAILS

Cell lines

HEK293 (female), HEK293T (female) MCF7 (female), U-373 MG (female), MDA-MB-468 (female), HT-29 (female), SW480 (male), HeLa (female) and MCF10A (female) cells were obtained from ATCC (American Type Culture Collection, Manassas, VA, USA). JHUEM7 (female) cells were obtained from RIKEN (Tsukuba, Ibaraki, Japan). HEC59 (female) cells were obtained from JCRB Cell Bank (Osaka, Ibaraki, Japan). NCM460D (male) cells were obtained from INCELL (Gangnam, Seoul, Republic of Korea). HEK293, HEK293T, MDA-MB-468, MCF7, and U-373 MG cells were cultured in high-glucose DMEM supplemented with 10% FBS and 2 mM glutamine. JHUEM7, HT-29, NCM460D and HEC59 cells were cultured in RPMI1640 supplemented with 1× non-essential amino acid (Gibco) and 10% FBS. SW480 and MCF10A cells were cultured in DMEM/F-12 supplemented with 1× non-essential amino acid, 2 mM glutamine and 10% FBS. HeLa cells were cultured in MEM supplemented with 10% FBS and 2 mM glutamine. Cells were grown on 100 × 20 mm culture plate (SPL) to 80% confluence. All cell lines were maintained at 37°C and 5% CO_2. All cell lines were obtained from certified vendors, authenticated, and confirmed to be mycoplasma-free prior to use.

Animals

BALB/c nude mice (CAnN.Cg-Foxn1nu/Crl, female, 8–12 weeks old) were purchased from OrientBio (Seongnam, Republic of Korea). The mice were maintained on a 12 h light/dark cycle in a temperature- and humidity-controlled facility, with *ad libitum* access to food and water. All mice care and use procedures were performed in accordance with the Guide for the Care and Use of Laboratory Animals and were approved by the Institutional Animal Care and Use Committee (IACUC) of Korea Advanced Institute of Science and Technology Animal Care and Use Committee (KA2025-059-v2.1).

METHOD DETAILS

LC-MS profiling of metabolites

Mass spectrometric analysis of the cell extracted samples was performed in a negative mode on a 1260 Infinity Quaternary Liquid Chromatography system equipped with a 6530 Q-TOF mass spectrometer (Agilent). Agilent MassHunter LC/MS Data Acquisition software (version B.05.00) was used for data collection. The mobile phases for liquid chromatography were water (A) and acetonitrile (B). Chromatography solvent system used was: 0–8 min (linear gradient): 0% solvent B to 100%, 8–10 min (isocratic): 100% solvent B. A 10 μL of sample dissolved in methanol was injected to a reversed-phase analytical column (Kinetex 2.6 μm XB-C18, 100 Å, 50 × 2.10 mm) with a flow rate of 0.5 mL/min. Typical sample ESI condition was set at nozzle voltage 1.0 kV, gas temperature 325°C, drying gas 10 L/min, nebulizer 20 psig, VCap 4000 V, fragmentor 100 V and skimmer 65 V. All LC-MS data was deconvoluted into individual chemical peaks by the MassHunter Qualitative Analysis Software B.05.00. The data files were transformed to CEF format files using DA reprocessor (Agilent, B.05.00). Subsequent statistical evaluation of independent pairs of groups were performed using Mass Profiler Professional software (Agilent, version 12.1) by unpaired *t* test analysis (cut-off value of $p < 1.0$, cut-off value of fold change >1.0). The p value <0.05 in the *t* test was defined as significant. The features found in LC/MS data file was 20 filtered based on an abundance filtering (minimum absolute abundance: 1000 counts) and number of ions (minimum number: 1). Percentile shift (value 75.0) was used as normalization algorithm option to compute the 75th percentile of the abundance values across all entities. ID Browser identification was conducted with a matching elemental formula by Agilent Masshunter ID Browser software B.05.00 using MassHunter METLIN Metabolite PCDL (Personal Compound Database and Library) file as a database.

HDX-MS analysis

The protein sequence coverage map was obtained from undeuterated controls as follows: 3.5 μL of 50 μM mTOR C-terminal fragment in 25 mM HEPES, pH 7.4, 50 mM KCl, 10 mM $MgCl_2$, 10% glycerol was diluted 96.5 μL of ice-cold quench (100 mM Glycine, 25 mM TCEP, pH 2.5). The quenched samples were injected into a Waters HDX nanoAcquity UPLC (Waters) with in-line pepsin digestion (Waters Enzymate BEH pepsin column). Peptic fragments were trapped on an Acquity UPLC BEH C18 peptide trap and separated on an Acquity UPLC C18 column. A 7 min, 5%–35% acetonitrile (0.1% formic acid) gradient was used to elute peptides directly into a Waters Synapt G2 mass spectrometer (Waters). MSE data were acquired with a 20 to 30 V ramp trap CE for high energy acquisition of product ions as well as continuous lock mass (Leu-Enk) for mass accuracy correction. Peptides were identified using the ProteinLynx Global Server 2.5.1 (PLGS) from Waters. Further filtering of 0.3 fragments per residues was applied in DynamX 3.0. HD exchange reactions, quenching and injection were performed using a using a LEAP autosampler controlled with HDxDirector. Briefly, 3.5 μL of ∼50 μM mTOR C-terminal fragment in 25 mM HEPES, pH 7.4, 50 mM KCl, 10 mM $MgCl_2$, 10% glycerol, 1% DMSO with or without 130 μM 13-*S*-HODE (Cayman Chemical) was incubated in 31.5 μL of 25 mM HEPES, 99.99% D_2O, pD 7.4, 50 mM KCl, 10 mM $MgCl_2$, 1% DMSO with or without 130 μM 13-*S*-HODE. All reactions were performed at 25°C. Prior to injection, deuteration reactions were quenched at various times (10 s, 1 min, 10 min, and 2 h) with 65 μL of ice-cold 100 mM Glycine buffer, 5 mM TCEP pH 2.5. Back exchange correction was performed against fully deuterated controls acquired by incubating 3.5 μL of 50 μM of mTOR C-terminal fragment in 31.5 μL 25 mM HEPES, 99.99% D_2O, pD 7.4, 50 mM KCl, 10 mM $MgCl_2$, containing 6 M deuterated Guanidine DCl for 2 h at 25°C prior to quenching. All deuteration time points were acquired in triplicates.

The deuterium uptake by the identified peptides through increasing deuteration time and for the fully deuterated control was determined using Water's DynamX 3.0 software. The normalized percentage of deuterium uptake (%D) at an incubation time t for a given peptide was calculated as follows: $\%D = (100(m_t\text{-}m_0))/(m_f\text{-}m_0)$. With m_t the centroid mass at incubation time t, m_0 the centroid mass of the undeuterated control, and m_f the centroid mass of the fully deuterated control. Percent deuteration difference plots (Δ%D) were generated using the percent deuteration calculated. Confidence intervals for the Δ%D plots were determined[55] and adjusted to percent deuteration using the fully deuterated controls. This approach involves the use of a two-criteria condition for determining the statistical significance of deuterium uptake differences observed for any given peptide: first, a difference in deuterium uptake at any single deuterium incubation time point (in colors) which is superior to the 98% confidence interval (dashed horizontal lines in Figures S2B and S2C) as determined using the overall standard deviation from the entire dataset (all peptides, all time points, all states). Second, a summed difference in deuterium uptake integrated over all time points probed which is superior to its respective 98% confidence interval (dash-dot horizontal line in Figure S2C) as determined using the overall standard deviation propagated to the number of time point.

Molecular modeling

The 13-*S*-HODE used for this study was created as a 2D structure by ChemBioDraw (ver. 11.0.1) and transferred to Chem3D Pro (ver. 11.0.1) to generate 3D structure. The structure of 13-*S*-HODE was saved as mol file format. The generated mol file transferred to Discovery Studio 3.0 (DS 3.0, Accelrys Inc., USA). The process of ligand preparation and optimization was performed by Prepare Ligands Module in DS 3.0. The PDB coordinates of human mTOR (PDB ID: 5FLC) were downloaded from the Protein DataBank.[33] Before conducting docking studies, water molecules were removed from the protein-ligand complexes and side chain bumps of amino acid residues were fixed. Hydrogen atoms were added by application of CHARMm Force Field, and Momany-Rone partial charge settings were used as default settings in DS 3.0. The potential binding site of 13-*S*-HODE in the ATP-biding site of mTOR was assigned to a spherical region with a radius of 20 Å from the key amino acids consisting of the ATP-binding site (Lys2187, Glu2190, His 2340, Asn2343, and Asp2357). Docking studies of 13-*S*-HODE were performed using CDOCKER protocol implemented in DS 3.0 by modifying default settings slightly (top hits: 100, random conformations: 10, orientations to refine: 10, simulated annealing: true, Force field: CHARMm, Grid extension: 8.0, Ligand partial charge method: Momany-Rone). The best-docked pose of 13-*S*-HODE was analyzed and visualized by using the PyMOL software.

Fluorescence-based thermal shift assay

The thermal shift assays were performed using the 7500 Real-Time PCR System (Applied Biosystems) melting curve program with a temperature increment of 1.0°C and a temperature range of 25°C–95°C. All reactions were incubated in a 20 μL final volume and assayed in 96-well plates using 1:1,000 dilution of 5,000 × SYPRO Orange stock solution (Sigma-Aldrich) and indicated concentrations (1.0 μM) of recombinant mTOR kinase domain diluted in buffer containing 10 mM HEPES·HCl pH 7.5. 13-*S*-HODE was added to the reaction to assess ligand-dependent thermal destabilization of mTOR kinase domain protein. The ligands (dissolved in DMSO) were incubated with mTOR kinase domain protein at 4°C for 25 min before acquiring the melting curves.[56] The T_m is identified by plotting the first derivative of the fluorescence emission as a function of temperature (−dF/dT) using GraphPad PRISM 8.0 software.

Generation of stable cell lines

The plasmid pCDH-MCS-T2A-copGFP-MSCV (System Biosciences; CD525A-1) was used as a backbone for expression of genes of interest. Lentiviruses were generated in HEK 293 T cells by transfecting the lentiviral plasmids together with packaging vectors (pRSV-Rev, pMDLg/pRRE) and envelop plasmid (pMD2.G) as manufacturer's protocol. Lentiviruses were added to MCF7 and HEK293T cells for 24 h and the transduced cells were selected by flow cytometry.

Cell lysis, immunoprecipitation, and immunoblotting

Cells were lysed in NP-40 lysis buffer (50 mM Tris-HCl at pH 7.5, 150 mM NaCl, 1% NP-40 substitute, 1 mM EDTA at pH 8.0, 50 mM NaF, 10 mM Na-pyrophosphate, 15 mM Na_3VO_4, and protease inhibitor cocktail (Roche)). Whole cell lysates were mixed with 5× SDS-sample buffer to a final concentration of 1–2 μg/μL, boiled for 5 min, and then used directly for immunoblotting or frozen at −20°C. For mTOR immunoprecipitations, the cells were treated as with the glutathione pulldown, except they were lysed/washed in CHAPS lysis buffer (40 mM HEPES at pH 7.4, 120 mM NaCl, 2 mM EDTA, 0.3% CHAPS, 50 mM NaF, 10 mM Na-pyrophosphate, and protease inhibitor cocktail (Roche)) and incubated with FLAG-M2-coupled agarose beads for 2 h at 4°C. For immnunoblotting, 10–50 μg of whole cell lysates, or 10–30 μL of FLAG-M2 immunoprecipitates were loaded into lanes of 4–12% bis-tris SDS-PAGE gels, run at 120 volts for 2 h in 1× glycine buffer, and then transferred to 0.45 μm nitrocellulose membrane at 60 volts for 2 h in 1× transfer buffer (1× glycine buffer without SDS, 20% methanol). The membranes were then immunoblotted for the indicated proteins. All primary antibodies were diluted 1:1000 in 5% BSA W/V TBST, except for GAPDH and FLAG antibodies which were diluted 1:2000. All secondary antibodies were diluted 1:5000 in 5% skim milk W/V TBST. Representative and replicate immunoblot data are shown in Data S1.

In vitro mTOR kinase assay

For *in vitro* mTOR kinase assay in Figure 3F, HEK293 cells were used to immunoprecipitate endogenous mTOR complexes. For mTORC1 and C2 kinase assays in Figures 2A and 2B, myc-raptor or myc-rictor was transfected in HEK293T cells for 48 h with

Flag-tagged mTOR. Cells were rinsed once with ice-cold PBS and lysed in ice-cold CHAPS lysis buffer. Cell lysates were incubated at 4°C for 10 min and the supernatant was collected by centrifuging lysates at 13,000 rpm for 10 min 2 μg of mTOR or FLAG antibody were added to the 2 mg of cell lysates and incubated with rotation for 2 h at 4°C. 20 μL of agarose beads (Pierce) were added and the incubation continued for 1 h mTOR or FLAG immunoprecipitates were washed twice with the same lysis buffer and twice with kinase wash buffer (25 mM HEPES at pH 7.4, 20 mM potassium chloride, 1 mM magnesium chloride). mTORC1 kinase assays were performed for 15 min at 37°C in a final volume of 15 μL of mTORC1 kinase buffer (25 mM HEPES at pH 7.4, 50 mM KCl, 10 mM $MgCl_2$, 500 μM ATP) and 150 ng of S6K1 as a substrate. Full-length S6K1 proteins were prepared as described previously.[22] HEK293T cells were transfected with HA-GST-p70S6K1 containing a PreScission protease cleavage site between the GST tag and S6K1. After 48 h, cells were treated with 20 μM LY294002 for 1 h. S6K1 was purified by using a glutathione bead column, followed by PreScission protease treatment. GST-fused S6K1 (amino acids 332–421) proteins were also purified. GST-S6K1 (331–321) cDNA was cloned, expressed in *Escherichia coli*, purified using glutathione beads, and cleaved of the GST-tag as described previously.[53] mTORC1 kinase reactions were stopped by the addition of 10 μL of sample buffer and boiling for 5 min and analyzed by SDS-PAGE and immunoblotting. *In vitro* mTORC2 kinase assay was performed by using mTORC2 kinase buffer (25 mM HEPES at pH 7.5, 100 mM potassium acetate, 1 mM $MgCl_2$, 500 μM ATP) with 100 ng of Akt1 as a substrate.

In vitro kinase assays for PI3KC3, DNA-PK, Erk

Kinase assays were performed by Reaction Biology Corporation. For *in vitro* PI3KC3 kinase assay, 50 μM PI:PS was used as a substrate, and the ADP production was quantified by ADP-Glo luminescence detection. Both DNA-PK and Erk kinase reaction buffers include 20 mM HEPES (pH 7.5), 10 mM $MgCl_2$, 1 mM EGTA, 0.02% Brij35, 0.02 mg/mL BSA, 0.1 mM Na_3VO_4, 2 mM DTT, and 1% DMSO. To measure DNA-PK activity, 20 μM peptide substrate [EPPLSQEAFADLWKK], 10 μg/mL DNA, and 10 μM ATP were used. For *in vitro* Erk kinase assay, 20 μM myelin basic protein and 10 μM ATP were used. ^{33}P-ATP (specific activity 10 μCi/μL) into the reaction mixture to initiate the reaction. After 2 h of reaction at room temperature, radioactivity was measured by filter-binding method. Kinase activity data were expressed as the percent remaining kinase activity in test samples compared to vehicle (DMSO) reactions.

Cellular thermal shift assay

Cellular thermal shift assay (CETSA) was performed to evaluate the interaction between 13-*S*-HODE and mTOR and to assess the compound's effect on mTOR stability under lysate conditions. Briefly, 2×10^6 cells were seeded in 100 × 20 mm culture dishes and cultured for 24 h. Cells were then transfected with 5 μg of FLAG-mTOR^{WT} or FLAG-mTOR$^{K2187A/E2190A}$ (kinase-dead mutant) plasmids using the jetPRIME transfection reagent (Polyplus), according to the manufacturer's protocol. After 48 h of transfection, cells were washed with PBS, detached with trypsin, and collected by centrifugation at 1500 rpm for 3 min. The cell pellets were resuspended in 500 μL of 0.3% CHAPS lysis buffer (40 mM HEPES pH 7.4, 120 mM NaCl, 2 mM EDTA, 0.3% CHAPS, 50 mM NaF, 10 mM Na-pyrophosphate) containing protease inhibitor cocktail (Roche, Switzerland). The lysates were incubated with gentle rotation for 20 min at 4°C and then centrifuged at 13,000 rpm for 20 min at 4°C to obtain the soluble fractions. For the treatment group, 13-*S*-HODE was added to the supernatant (2 mg/mL total protein) to a final concentration of 135 μM and incubated for 1 h at 4°C. Subsequently, aliquots of the treated lysates were transferred to PCR tubes and heated at 37°C, 48°C, and 50°C for 5 min, followed by centrifugation at 13,000 rpm for 20 min. Soluble proteins were collected from the supernatant and subjected to Western blot analysis. Equal amounts of protein were separated on 8% SDS-PAGE gels and transferred onto nitrocellulose membranes. The membranes were probed with anti-FLAG (Merck, F1804), and anti-β-actin (Cell Signaling Technology, 4970) at 4°C overnight. After washing with TBST, membranes were incubated with HRP-conjugated secondary antibodies (Cell Signaling Technology, USA) for 1 h at 37°C. Immunoreactive bands were detected using an enhanced chemiluminescence system (ECL; Bio-Rad, USA), and protein band intensities were quantified using ImageJ software.

Biotin-labeled 13-*S*-HODE pulldown assay

HEK293T cells were lysed in CHAPS lysis buffer used for mTORC immunoprecipitation. 2 mg of total cell lysates were incubated with 10 μM of biotinylated 13-*S*-HODE (Cayman Chemical) or linoleic acid (Sigma-Aldrich). For competition, 20 μM of non-biotinylated 13-*S*-HODE or linoleic acid were pre-incubated with cell lysates before binding. Streptavidin beads were added to the reaction mixture, and the assay was assessed by immunoblotting. To map 13-*S*-HODE–mTOR binding, HEK293T cells were transfected with the FLAG-mTOR^{WT}, mTOR^{D2195A} or mTOR$^{K2187A/E2190A}$ and then lysed in CHAPS lysis buffer. 2 mg of cell lysates were incubated with 20 μL of beads conjugated with an antibody against FLAG (Sigma-Aldrich) or Rabbit TrueBlot: Anti-Rabbit IgG HRP beads (Rockland)for 18 h at 4°C with agitation. Then, beads were washed and incubated with or without unlabeled 13-*S*-HODE in the presence of biotinylated 13-*S*-HODE.

Measurement of cellular 13-*S*-HODE by LC-MS/MS

13-*S*-HODE was extracted from ∼1.4 mL cell supernatant using solid phase extraction (SPE). 60 mg Oasis HLB (Waters) SPE cartridge was washed and preconditioned with ethyl acetate, methanol, and (0.1% acetic acid + 5% MeOH) in H_2O, sequentially. 10 μL of 0.2 mg/mL of EDTA and BHT in MeOH: H_2O (50:50) was added to sorbent bed of an SPE column. Equal volume of (0.1% acetic acid + 5% MeOH) in H_2O was added to the cell supernatant. 50 μL of 500 nM 13-*S*-HODE-d4 was also added as internal standard into a sample solution. The solution was added into SPE column. The column was washed with 2 column volumes of (0.1% acetic

acid + 5% methanol) in H_2O, then the column was dried using vacuum. Finally, 13-*S*-HODE was eluted with 0.5 mL methanol followed by 1.5 mL ethyl acetate. The sample solution was dried using vacuum centrifuge, then stored at −20°C until analysis. The dried matter was reconstituted with 40 μL of methanol prior to LC-MS/MS analysis.

13-*S*-HODE was determined using an LC-MS/MS system equipped with Agilent 1290 HPLC (Agilent) and QTRAP 5500 mass spectrometry (AB Sciex). A reverse-phase column (Pursuit5 C18, 150 × 2.1 mm) was used with mobile phase A (0.1% acetic acid in H_2O) and mobile phase B (0.1% acetic acid in acetonitrile/methanol (84/16)). The LC was run at 250 μL/min and 35°C. The separation gradient was as follows: 35% B at 0 min, hold at 35% B for 0.25 min, 35 to 45% of B for 0.75 min, hold at 45% of B for 2 min, 45 to 56% of B for 5.5 min, 56 to 65% of B for 5.5 min, hold at 65% of B for 6 min, 65 to 95% of B for 1.5 min, hold at 95% of B for 5.5 min, 95 to 35% of B for 0.1 min, and then hold at 35% of B for 2.9 min. The multiple reaction monitoring (MRM) mode was performed in negative ion mode for 13-*S*-HODE, and the extracted ion chromatogram corresponding to the specific transition of 13-*S*-HODE was used for quantification (Q1/Q3 = 295/195, RT = 18.09 min for 13-*S*-HODE; Q1/Q3 = 299/198, RT = 17.93 min for 13-*S*-HODE-d4). The calibration range for 13-HODE was 1–10000 nM (r2 ≥ 0.99). Data analysis was performed by using either Analyst 1.5.2.

Cell proliferation and colony formation assay

MDA-MB-468, JHUEM7 (5×10^3 cells/mL), MDA-MB-231, MCF7 (1×10^4 cells/mL) were seeded into 96-well culture plates. After overnight incubation, cells were treated with DMSO or 135 μM of 13-*S*-HODE for various times. Then 20 mL 3-(4,5-dimethylthiazol-2-yl)-2,5-diphenyl tetrazolium bromide (MTT) solution (2.5 mg/mL in PBS) was added to each well, and the plates were incubated for an additional 1 h at 37°C. The optical density of each well was measured at 492 nm with a SpectraMax Paradigm Reader (Molecular Devices). For colony formation assay, cells (4×10^4/well) were seeded into 24-well plates and cultured overnight before being incubated with DMSO or 135 μM of 13-*S*-HODE for 4 days. The resulting colonies were fixed with methanol at −20°C for 30 min and were stained with 1% crystal violet for 15 min.

Organic synthesis of 13-*S*-HODE

13-*S*-HODE (>95% *ee*) was prepared by the previously described synthetic method (Figure S6 and Data S2).[57] All the chemicals and solvents used in the reaction were purchased from Sigma-Aldrich, TCI, or Alfa Aesar and were used without further purification. All reactions were carried out in oven-dried glassware under an inert atmosphere and reaction temperature was controlled by an oil bath. Reactions were monitored by TLC on 0.25 mm Merck precoated silica gel plates (60 F254). Reaction progress was monitored by TLC analysis using a UV lamp and/or $KMnO_4$ staining or *p*-anisaldehyde staining solution for detection purposes. Column chromatography was performed on silica gel (230–400 mesh, Merck, Darmstadt, Germany). ^1H and ^{13}C NMR spectra were recorded at room temperature (298 K) in CDCl3 (7.26 ppm/77.16 ppm), CD_3OD (3.31 ppm/49.00 ppm) or CD_3CN/D_2O (2.53 and 4.79 ppm/1.32 and 118.26 ppm) on Bruker Ultrashield 600 MHz Plus spectrometer and referenced to an internal solvent. NMR solvents including $CDCl_3$, CD_3OD, CD_3CN, and D_2O were used as received from the Eurisotop company. Chemical shifts are reported in parts per million (ppm). Coupling constants (*J*) are given in Hertz. Splitting patterns are indicated as s, singlet; d, doublet; t, triplet; q, quartet; m, multiplet; dd, double of doublet; dt, double of triplet; br, broad for ^1H NMR data. High-resolution mass spectra (HRMS) were recorded on an Agilent 6530 Accurate mass Q-TOF LC/MS spectrometer. Reversed-phase high-performance liquid chromatography (RP-HPLC) purification using a semi-preparative column (Phenomenex Gemini-NX C18, 110 Å, 150 mm × 10 mm, 5 μm) was performed on Agilent 1260 Infinity (Agilent). The purity of all final compounds was measured by analytical RP-HPLC on an Agilent 1260 Infinity (Agilent) with a C18 column (Phenomenex, 150 mm × 4.6 mm, 3 μm, 110 Å) using water (containing 0.1% FA) and acetonitrile (ACN; containing 0.1% FA) as mobile phase. All compounds were monitored at a UV detector: 220 nm. The purities of the tested compounds were >95%. Melting point (mp) was measured using a Q2000 DSC (TA Instruments, New Castle, DE). Optical rotation was measured at λ = 589 nm, corresponding to the sodium D line, at the indicated temperature using a Krüss P8000 polarimeter.

(*E*)-1-Methoxy-4-((non-3-en-1-yloxy)methyl)benzene (1)

To a solution of (E)-non-3-en-1-ol (8.0 g, 56.2 mmol) in THF (160 mL) were added NaH (60%, 3.14 g, 78.7 mmol), PMBCl (9.0 mL, 66 mmol) and tetra-*n*-butylammonium bromide (187 mg, 0.56 mmol). The reaction mixture was heated at reflux for 24 h. After cooling to room temperature, the reaction mixture was poured into saturated aqueous NH_4Cl solution and extracted with ethyl acetate. The organic layer was washed with water and brine, dried over $MgSO_4$, filtered, and concentrated under reduced pressure. The residue was purified by column chromatography on silica gel using Hex/EtOAc (98:2) to afford compound 1 as a colorless oil (12.0 g, 81%). R_f = 0.25 (Hex/EtOAc (98:2), $KMnO_4$-stain); 1H NMR (600 MHz, $CDCl_3$) δ 7.26 (d, *J* = 8.58 Hz, 2H), 6.88 (d, *J* = 8.64 Hz, 2H), 5.49 (dt, *J* = 15.3, 6.7 Hz, 1H), 5.41 (dt, *J* = 15.3, 6.7 Hz, 1H), 4.45 (s, 2H), 3.81 (s, 3H), 3.45 (t, *J* = 7.0 Hz, 2H), 2.30 (q, *J* = 6.7 Hz, 2H), 1.98 (q, *J* = 6.7 Hz, 2H), 1.38–1.23 (m, 6H), 0.89 (t, *J* = 6.9 Hz, 3H); $^{13}C\{^1H\}$ NMR (151 MHz, CDCl3) δ159.3, 132.8, 130.9, 129.4, 129.4, 126.4, 114.0, 114.0, 72.7, 70.2, 55.5, 33.3, 32.8, 31.6, 29.4, 22.8, 14.3.

(3*S*,4*S*)-1-((4-Methoxybenzyl)oxy)nonane-3,4-diol (2)

A mixture of $K_3[Fe(CN)_6]$ (18.7 g, 57.2 mmol, 3.0 equiv), K_2CO_3 (7.88 g, 57.2 mmol, 3.0 equiv) and $(DHQ)_2PHAL$ (142.6 mg, 0.19 mmol, 1.0 mol %) in t-BuOH·H_2O (1:1, 200 mL) was cooled to 4°C. $K_2OsO_4 \cdot 2H_2O$ (28.8 mg, 0.076 mmol, 0.4 mol %) was then added, followed by methanesulfonamide (1.80 g, 19.0 mmol, 1.0 equiv). After stirring for 5 min at 4°C, compound 1 (5.0 g, 19.0 mmol) was added in one portion. The reaction mixture was stirred at 4°C for 24 h and then quenched with solid Na_2SO_3 (3.6 g, 28.6 mmol,

1.5 equiv). Stirring was continued for an additional 45 min and the solid was removed by vacuum filtration. The filtrate was extracted with EtOAc (3 × 100 mL), and the combined organic layers were washed with brine, dried over $MgSO_4$, filtered, and concentrated under reduced pressure. The residue was purified by column chromatography on silica gel using Hex/EtOAc (3:1) to give the crude 2 as a white solid, which was further purified by recrystallization in Hex/EtOAc (20:1) to afford the desired pure product 2 as a white solid (3.59 g, 79%, 95% *ee*). The enantiomeric ratio was determined by chiral HPLC [250 mm × mm, 5 μm, Daicel Chiralpak-IG, 90:10 to 0:100 hexane/MTBE containing 0.05% glacial acetic acid, 1.0 mL/min, 220 nm, t_R = 10.7 min [97.8%, (*S,S*)-isomer], 11.5 min [2.2%, (*R,R*)-isomer]. mp 40−41°C; R_f = 0.25 (Hex/EtOAc (7:3), $KMnO_4$-stain); ^{1}H NMR (600 MHz, $CDCl_3$) 7.24 (d, *J* = 8.6 Hz, 2H), 6.88 (d, *J* = 8.6 Hz, 2H), 4.46 (s, 2H), 3.80 (s, 3H), 3.71–3.62 (m, 3H), 3.41 (m, 1H), 3.19 (d, *J* = 3.9 Hz, 1H), 2.52 (d, *J* = 8.4 Hz, 1H), 1.90–1.70 (m, 2H), 1.51–1.23 (m, 8H), 0.89 (t, *J* = 7.0 Hz, 3H); ^{13}C{^{1}H} NMR (151 MHz, $CDCl_3$) δ 159.6, 130.0, 129.6, 129.6, 114.1, 114.1, 74.5, 73.9, 73.3, 68.5, 55.5, 33.7, 33.4, 32.1, 25.6, 22.8, 14.2; HRMS (ESI) m/z: [M + Na]+ calculated for $C_{17}H_{28}O_4Na^+$ 319.1880; Found 319.1856.

(4*S*,5*S*)-4-(2-((4-Methoxybenzyl)oxy)ethyl)-5-pentyl-1,3-dioxolan-2-one (3)

The compound 2 (3.5 g, 11.8 mmol) was dissolved in dimethyl carbonate (1.5 mL, 17.7 mmol, 1.5 equiv) and K_2CO_3 (98 mg, 0.71 mmol, 0.06 equiv) was added as a catalyst. The resulting mixture was stirred at 85°C for 3 h. Methanol and excess dimethyl carbonate were then removed under reduced pressure at 30°C. The residue was purified by column chromatography on silica gel using Hex/EtOAc (9:1) to afford compound 3 as a colorless oil (3.48 g, 91%). R_f = 0.25 (Hex/EtOAc (9:1), $KMnO_4$-stain); ^{1}H NMR (600 MHz, $CDCl_3$) δ 7.22 (d, *J* = 8.6, 2H), 6.88 (d, *J* = 8.6, 2H), 4.45–4.39 (m, 3H), 4.33 (m, 1H), 3.80 (s, 3H), 3.60–3.57 (m, 2H), 2.00–1.94 (m, 2H), 1.70–1.59 (m, 2H), 1.49–1.23 (m, 6H), 0.88 (t, *J* = 7.0 Hz, 3H); ^{13}C{^{1}H} NMR (151 MHz, $CDCl_3$) δ 159.5, 154.8, 130.0, 129.6, 129.6, 114.0, 114.0, 82.4, 79.8, 73.2, 65.2, 55.4, 34.2, 33.8, 31.4, 24.4, 22.5, 14.1; HRMS (ESI) m/z: $[M + Na]^+$ calculated for $C_{18}H_{26}O_5Na^+$ 345.1672; Found 345.1639.

(4*S*,5*S*)-4-(2-Hydroxyethyl)-5-pentyl-1,3-dioxolan-2-one (4)

To a stirred solution of 3 (3.3 g, 10.2 mmol) in a mixture of DCM (40 mL) and H_2O (2 mL) was added DDQ (3.47 g, 15.3 mmol, 1.5 equiv) at 4°C. After 30 min, the mixture was diluted with water and extracted with DCM. The organic layer was washed with water and brine, dried over $MgSO_4$, filtered, and concentrated under reduced pressure. The residue was purified by column chromatography on silica gel using Hex/EtOAc (8:2) to afford compound 4 as a colorless oil (1.7 g, 83%). R_f = 0.25 (Hex/EtOAc (7:3), $KMnO_4$-stain); ^{1}H NMR (600 MHz, $CDCl_3$) δ 4.48 (m, 1H), 4.35 (m, 1H), 3.81 (m, 2H), 2.14 (br s, 1H), 1.98–1.88 (m, 2H), 1.77–1.65 (m, 2H), 1.51–1.27 (m, 6H), 0.88 (t, *J* = 6.96 Hz, 3H); ^{13}C{^{1}H} NMR (151 MHz, $CDCl_3$) δ 155.0, 82.5, 79.7, 58.2, 36.3, 33.6, 31.5, 24.4, 22.5, 14.1; HRMS (ESI) m/z: $[M + H]^+$ calculated for $C_{10}H_{19}O_4^+$ 203.1278; Found 203.1263.

(*S,E*)-4-hydroxynon-2-enal (5)

To a stirred solution of compound 4 (100 mg, 0.49 mmol) in EtOAc (10 mL) was added 2-Iodoxybenzoic acid (IBX, 45% w/w with stabilizer) (609 mg, 0.98 mmol, 2.0 equiv) under an argon atmosphere. The resulting suspension was refluxed for 3–4 h (TLC monitoring). The reaction was cooled to room temperature and the solid was removed by vacuum filtration. The filtrate was washed with saturated aqueous $NaHCO_3$, brine, dried over $MgSO_4$, filtered, and concentrated under reduced pressure. The residue was purified by flash chromatography on silica gel using DCM/EtOAc (98:2) as eluent to afford the compound 5 (63 mg, 82%) as a colorless oil. R_f = 0.25 (DCM:EtOAc, 98:2. $KMnO_4$-stain); ^{1}H NMR (600 MHz, $CDCl_3$) δ 9.57 (d, *J* = 7.8 Hz, 1H), 6.82 (dd, *J* = 15.7, 4.8 Hz, 1H), 6.30 (ddd, *J* = 15.7, 7.8, 1.6 Hz, 1H), 4.42 (q, *J* = 4.8 Hz, 1H), 2.01 (s, 1H), 1.68–1.57 (m, 2H), 1.49–1.41 (m, 1H), 1.41–1.35 (m, 1H), 1.35–1.26 (m, 4H), 0.89 (t, *J* = 7.0 Hz, 3H); ^{13}C{^{1}H} NMR (151 MHz, $CDCl_3$) δ 193.9, 159.3, 130.9, 71.3, 36.7, 31.8, 25.1, 22.7, 14.2; HRMS (ESI) m/z: $[M + H]^+$ calculated for $C_9H_{17}O_2^+$ 157.1223; Found 157.1226.

(8-Carboxyoctyl)triphenylphosphonium bromide (6)

Triphenylphosphine (5.9 g, 22.2 mmol, 1.5 equiv) was dissolved in freshly dried acetonitrile (90 mL) in a 100 mL round-bottomed flask. A solution of 9-bromononanoic acid (3.5 g, 14.8 mmol) in acetonitrile (10 mL) was added dropwise to the stirred triphenylphosphine solution. The reaction mixture was refluxed at 90°C for 48 h under an argon atmosphere and the solvent was removed under reduced pressure to afford the crude (8-carboxyalkyl)triphenylphosphonium bromide salts as a slightly yellow oil. Toluene (20 mL) was added to the residue, and the mixture was refluxed for 30 min. The toluene phase was decanted, and this washing process was repeated with toluene (20 mL). Anhydrous diethyl ether (30 mL) was added to the residue, and recrystallization at 4°C afforded a pale yellow solid. The solid was triturated with diethyl ether, filtered, and washed several times with diethyl ether. Drying under vacuum overnight afforded compound 6 as a white solid (7.48 g, 95%) without further purification. R_f = 0.1 (Hex:EtOAc 7:3). $KMnO_4$-stain); ^{1}H NMR (600 MHz, DMSO) δ 11.95 (s, 1H), 7.91–7.76 (m, 15H), 3.63–3.56 (m, 2H), 2.15 (t, *J* = 7.4 Hz, 2H), 1.51 (m, 2H), 1.48–1.40 (m, 4H), 1.25 (m, 2H), 1.22–1.14 (m, 4H); ^{13}C{^{1}H} NMR (151 MHz, DMSO) δ 174.4, 134.9, 133.6, 130.2, 118.9, 118.3, 33.6, 29.7, 29.6, 28.4, 27.9, 24.4, 21.7, 20.3; HRMS (ESI) m/z: $[M]^+$ calculated for $C_{27}H_{32}O_2P^+$ 419.2134; Found 419.2146.

(*S*,9*Z*,11*E*)-13-hydroxyoctadeca-9,11-dienoic acid, 13-(*S*)-HODE (7)

(8-carboxyoctyl)triphenylphosphonium bromide 6 (1.43 g, 2.88 mmol, 1.5 equiv) was suspended in anhydrous N,N′-Dimethylpropyleneurea (DMPU) (5 mL) under an argon atmosphere. A 1.5 M lithium bis(trimethylsilyl) amide (LiHMDS) solution in THF (6.14 mL, 9.22 mmol, 4.80 equiv) was added dropwise over 40 min at 0°C, and the mixture was stirred at 0°C for an additional

15 min. The resulting dark red solution was maintained to 0°C and a solution of (*S,E*)-4-hydroxynon-2-enal 5 (300 mg, 1.92 mmol) in THF (2 mL) was added dropwise over 40 min. The reaction mixture was then allowed to warm to room temperature and stirred for 8 h (monitored by TLC). The reaction was quenched with 1.0 M aqueous HCl until pH < 2. The aqueous layer was extracted with EtOAc (3 × 40 mL), and the combined extracts were dried over $MgSO_4$, filtered, and concentrated under reduced pressure. The crude mixture was purified by column chromatography using hexane/diethyl ether (8:2) containing 1% glacial acetic acid to give (*S*,9*Z*,11*E*)-13-hydroxyoctadeca-9,11-dienoic acid 7 as a colorless oil in an 8:2 (*Z*/*E*) ratio (192 mg, 34%, 95% *ee*). R_f = 0.25 (Hex/Ether (8:2) with 0.1% AcOH, $KMnO_4$-stain); The enantiomeric ratio was determined by chiral HPLC [250 mm × 4.6 mm, 5 μm, Daicel Chiralpak-IG, 80:20 to 0:100 hexane/MTBE containing 0.05% glacial acetic acid, 1.0 mL/min, 220 nm, t_R = 6.4 min [2.5%, (*R,R*)-isomer], 11.6 min [97.5%, (*S,S*)-isomer]. $[\alpha]_D^{28}$ = +10.8 (c 1.0, $CHCl_3$); ^{1}H NMR (600 MHz, $CDCl_3$) δ 6.49 (dd, *J* = 15.2, 10.8 Hz, 1H, H-11), 5.97 (t, *J* = 10.8 Hz, 1H, H-10), 5.66 (dd, *J* = 15.2, 6.8 Hz, 1H, H-12), 5.44 (dt, *J* = 10.8, 7.2 Hz, 1H, H-9), 4.17 (q, *J* = 6.8 Hz, 1H), 2.34 (t, *J* = 7.4 Hz, 2H), 2.20–2.15 (m, 2H), 1.66–1.60 (m, 2H), 1.55 (m, 2H), 1.41–1.36 (m, 3H), 1.36–1.27 (m, 11H), 0.89 (t, *J* = 6.8 Hz, 3H); $^{13}C\{^1H\}$ NMR (151 MHz, $CDCl_3$) δ 179.2, 136.0, 133.1, 128.1, 126.1, 73.2, 37.5, 34.1, 32.0, 29.6, 29.1, 29.1, 29.0, 27.8, 25.3, 24.8, 22.8, 14.3; HRMS (ESI): $[M - H]^-$ calculated for $C_{18}H_{31}O_3^-$, 295.2278; found, 295.2289.

RNA-sequencing

Total RNA was isolated from cells using Tri reagent (Molecular Research Center) according to the manufacturer's protocol. 1 μg of total RNA was processed for preparing mRNA sequencing library using MGIEasy RNA Directional Library Prep Kit (MGI) according to manufacturer's instruction. The first step involves purifying the poly-A containing mRNA molecules using poly-T oligo attached magnetic beads. Following purification, the mRNA is fragmented into small pieces using divalent cations under elevated temperature. The cleaved RNA fragments are copied into first strand cDNA using reverse transcriptase and random primers. Strand specificity is achieved in the RT directional buffer, followed by second strand cDNA synthesis. These cDNA fragments then have the addition of a single 'A' base and subsequent ligation of the adapter. The products are then purified and enriched with PCR to create the final cDNA library. The double stranded library is quantified using QauntiFluor ONE dsDNA System (Promega). The library is circularized at 37°C for 30 min, and then digested at 37°C for 30 min, followed by cleanup of circularization product. To make DNA nanoball (DNB), the library is incubated at 30°C for 25 min using DNB enzyme. Finally, library was quantified by QauntiFluor ssDNA System (Promega). Sequencing of the prepared DNB was conducted on the MGIseq system (MGI) with 150 bp paired-end reads. The limma, edgeR, msigdbr, clusterProfiler packages in R, an open-source programming environment, was used to perform differentially expressed genes, gene set enrichment and pathway enrichment analysis. ENTREZID, MsigDB, GO terms and KEGG pathways were mapped and were used to perform enrichment test based on hypergeometric distribution. To prevent high false discovery rate (FDR) in multiple testing, *q*-values were also estimated for FDR control.

Mouse tumor xenograft studies

Animal protocols were performed in accordance with the guidelines approved by the Korea Advanced Institute of Science and Technology Animal Care and Use Committee. MDA-MB-468 (1×10^7 cells), JHUEM7 (5×10^6 cells) cells were implanted subcutaneously into the female BALB/c nude mice at the age of 8–12 weeks. After the mean tumor volumes reached 50 mm^3, the mice were randomly assigned into two different groups (6 mice/group). The body weight and tumor diameters were measured every other day. Tumor volume was assessed using calipers according to the formula $0.5\times (W)^2 \times (L)$, and a Student's *t* test was used to determine the *p* values. Mice received intratumoral or intravenous injections of 10 mg/kg 13-*S*-HODE every 2 days.

QUANTIFICATION AND STATISTICAL ANALYSIS

Quantification and statistical analyses were performed using GraphPad Prism version 8.0 (GraphPad Software, La Jolla, CA, USA). For the differences between two groups were examined using an un-paired two-sided Student's *t* test. For comparisons involving more than two groups, a one-way ANOVA was used. Post hoc testing was performed by with a Tukey's multiple comparisons test. In all cases, ns: not significant, $p \geq 0.05$; *$p < 0.05$; **$p < 0.01$; ***$p < 0.001$.